Investigation of Ferrosilicon produced with Si recovered from end-of-life photovoltaic panels.

Filip Kuśmierczyk, Mateusz Kopyściański, Adarsh Rai, Tomasz Kozieł, Marcin Goły, Agnieszka Kopia, Piotr Migas, Mirosław Karbowniczek, Pradeep Padhamnath*

AGH University of Krakow, al. Adama Mickiewicza 30, 30-059 Kraków, Poland

*ppadhamnath@agh.edu.pl

Abstract

Recycling end-of-life (EOL) silicon (Si) PV modules have gathered recent attention from researchers. PV modules can be recycled using a closed loop cycle where the materials recovered are reinjected into the supply chain for producing new modules. However, such solutions are extremely complex, expensive and could lead to further generation of harmful chemicals or emissions. Another way to recycle c-Si PV modules is by using them to produce other commercially important materials, for example ferrosilicon, using an easy and inexpensive route. Ferrosilicon is produced by reduction of silica using carbonaceous sources, which generates planet warming greenhouse gases. In this work, we present a simple method to use recycled Si (reSi) obtained from EOL PV modules to produce FeSi using induction furnace and no carbonaceous source. Along with reSi, metallurgical grade Si and commercial FeSi75 were also used to produce FeSi samples for comparison. FeSi samples with different silicon content were prepared. We also investigate the effect of the oxygen in the processing atmosphere, by preparing samples in arc furnace under argon atmosphere. The samples were characterized using scanning electron microscope coupled with Energy dispersive X-ray spectroscopy, to analyse the microstructure. X-ray diffraction was also used to identify and compare the phases formed in different samples. Hardness of the samples was also determined to understand the ease in the mechanical processing of the samples for potential commercial applications. Through the experimental results we have shown that silicon recovered from EOL PV panels could be used in the fabrication of FeSi.

1. Introduction

Silicon is widely used across various industries, including automotive, construction, and medicine, due to properties such as abundance, versatility, resistance to water and oxidation, and radiation shielding [1,2]. One of silicon's most significant uses of Si is as a semiconductor, which is essential for application in electronics. The demand for growth in photovoltaics (PV) deployment as a clean energy source in response to climate change, has further cemented the position of silicon in enabling energy transition [3,4]. Although photovoltaics is among the most promising technologies for sustainable energy production [4–6], optimal waste management for end-of-life solar panels remains challenging. In this context, efficient silicon recovery from electronics, especially from photovoltaic panels is increasingly critical [7–9].

According to the predictions published by International Renewable Energy Agency (IRENA), the cumulative PV panel waste could reach 1.7 - 8 million tons in 2030 and 60 – 78 million tons by 2050 for installed capacity of 4500 GW [10]. Given an average panel life of 25 years and the increased production and deployment of PV panels, large amounts of PV wastes are anticipated by early 2030s. It is expected that by 2040, the weight of waste PV panels generated would match that of the new installations [10].

Although silicon constitutes about 28% of the Earth's crust, it is most widely available in the form oxide (SiO_2), either as sand or quartz. The oxide is extremely stable and is often used as a refractory material. The extraction of Si its extraction from primary oxide employs significant carbon. Each kilogram of silicon metal (metallurgical grade) produced, accounts for approximately 6kg CO_2. This polysilicon is further refined and manufactured into single crystal ingots using Czochralski process, which further adds to the carbon emissions, depending on the source of the electricity used. Hence, recycling the Si from electronic waste, such as Si PV panels, can help greatly in reducing CO_2 emissions. Recycling just 1 ton of silicon photovoltaic panels can save up to 1,200 kg of CO_2 equivalent per kg compared to producing modules from raw materials [11]. Development of technologies for effective silicon recovery from end-of-life (EOL) or discarded photovoltaic panels is crucial for the management of electronic waste [12]. The discarded electronic waste could be viewed as a valuable resource for several raw and intermediate materials. This could offer substantial economic and ecological benefits, aligned with the sustainable development goals [13–15]. Although photovoltaic panels installed in early 2000s are prognosed to serve up to 40 years (with limited performance), most of them are discarded much earlier than their lifetime due to various reasons including damage and technology upgrade [16]. Therefore, there is an urgent need to develop technologies for recycling and managing the electronic waste, as the waste is expected to grow exponentially [9,17].

In general, there are two different recycling pathways to manage waste – closed loop recycling or cradle to cradle recycling and open loop recycling [18,19]. In closed loop recycling, the materials extracted from the waste are reused to make the same product after some processing. For example, the Si extracted from the EOL PV panels is purified and is used to make the solar cells which are then incorporated into the PV panels [[20,21] .Usually silicon recycling processes employ a number of mechanical, thermal chemical treatments, in various combinations [22]. Various chemicals such as H_3PO_4, HNO_3, HF and HCl are used for removing of impurities (including Ag, Al, Si compounds etc.) to ensure the purity of obtained product. However, this approach also generates problematic and potentially toxic gases and effluents [12,17,23]. While it is possible to obtain high purity silicon for further use in high end applications, in reality, the recovered silicon usually results in poor performance [24,25]. Further, despite the use of expensive and laborious techniques the content of impurities in silicon still might be significant, above 2% [26,27]. Further, in many places, silicon modules have been dumped in landfill sites and are no longer suitable for recovering Si and other precious metals, essentially rendering them non-recyclable, which can lead to additional soil and water pollution [28–30]. Therefore, it is essential to develop a method for recycling and cost-effective repurposing of EOL PV panels. The large quantity of silicon available globally

in discarded PV panels could be used to manufacture other valuable resources, which are comparatively less sensitive to the presence of metallic impurities. One such example is the use of EOL PV panels in producing ferrosilicon (FeSi) alloys.

FeSi alloys are broadly used in metallurgical industry for alloying, deoxidation and casting operations. FeSi is used as the main source of silicon in steels for spring and electrical applications [31,32]. Traditional silicon production from primary sources relies on coal and coke, generating approximately 4 tons of CO_2 per ton of FeSi, with additional emissions of SO_x, NO_x, and particulate matter [33,34]. Most of these carbon emissions originate from the carbonaceous reduction process of SiO_2. Recently some efforts have been made in using recycled sources of carbon for production of FeSi which could potentially reduce the overall carbon emissions [35], however, they still do not completely eliminate the emission of CO_2. Utilizing an alternative production method, such as arc or induction furnace, can significantly reduce these emissions by eliminating the need for carbon sources. Consequently, FeSi production via silicon recycling offers a promising pathway in addressing modern environmental challenges.

This study proposes an innovative approach that combines Si wafer recycling with FeSi production from secondary sources, contributing to efficient utilization of resources and hazardous emissions reduction. This method could offer an optimized alternative to silicon extraction from primary sources. Moreover, different production routes were compared. Additionally, the impact of source of silicon and its content on selected properties, as well as microstructure of obtained alloys was studied to demonstrate the broad applicability of this comprehensive recycling process.

1. Experimental Details

1.1. Raw materials used in this work.

In this work we have tried to understand the impact of the recycled Si content on the microstructure and formation of ferrosilicon alloys, while comparing it with commercially produced Si (metallurgical grade) and commercially procured FeSi75 (≈72% wt. Si). FeSi45 alloys were prepared by melting calculated amount of low-carbon, low alloyed iron (procured commercially) in an induction furnace and adding the Si after the steel had completely melted. This was done to prevent the formation of silicon carbide compounds, and to prevent further uncertainty in analysis. For all samples, the Si addition was done at a temperature between 1450-1500 C. Calculated and measured amount of low carbon steel was placed inside an alumina crucible which was then placed inside a larger graphite crucible. The alumina crucible was needed to prevent any reaction between the steel and Si with the carbon in the graphite crucible. The graphite crucible was used as a secondary heat source inside the induction furnace for the melting of Fe, Si and other constituents and for sustaining the required temperatures.

Three different sources of Si were used for the preparation of the FeSi; i) commercially procured metallurgical grade silicon (mgSi) ii) Commercially procured FeSi75 (FeSi75) iii) recycled silicon recovered from electronic waste (reSi). The recycled silicon was obtained by crushing and sorting to recover silicon from the end-of-life PV panels. The PV panels were crushed using an industrial crushing tool and the glass, plastic and other non-mechanical debris

were removed using mechanical process such as gravitational separation process and manual separation. The recovered silicon was then washed and dried in a thermal hot air oven at a temperature of 150 C for one hour. The chemical composition of the low carbon iron and the different sources of Silicon as determined by atomic emission spectroscopy (AES) are given in table 1-4.

FeSi alloys were prepared with three different Si concentrations – 10%, 20% and 45 %. They are referred throughout this work as FeSi10, FeSi20 and FeSi45. The experiment plan in terms of the mass of the different constituents are shown in table 5. The plan of the experiment was to keep the same amount (mass) of Fe and Si and to maintain the Fe/Si ratio in the final sample for each intended concentration. For example, the concentration of Si in mg-Si, FeSi75 and re-Si are 99.3%, 72.5% and 98.06% respectively. Therefore, the total weight of sample is slightly different for each source of silicon. The actual mass of the charge and the mass balance of the final sample obtained are shown later under the results and discussion session.

Table1: Elemental analysis of the steel used for fabricating FeSi samples.

Sr no.	Element (symbol)	Content [wt.%]
1	Aluminium (Al)	0.03
2	Carbon (C)	0.0018
3	Copper (Cu)	0.001
4	Lead (Pb)	0.005
5	Manganese (Mn)	0.07
6	Nickel (Ni)	0.017
7	Nitrogen (N)	0.0016
8	Phosphorus (P)	0.008
9	Silicon (Si)	0.003
10	Sulphur (S)	0.008
11	Tin (Sn)	0.0008
12	Zinc (Zn)	0.001
13	Iron (Fe)	99.85

Table2: Elemental analysis obtained of the FESi75 used for fabricating FeSi samples.

Sr no.	Element (symbol)	Content [wt.%]
1	Iron (Fe)	25.78
2	Silicon (Si)	72.5
3	Aluminium (Al)	1
4	Calcium (Ca)	0.29
5	Carbon (C)	0.14
6	Chromium (Cr)	0.028
7	Manganese (Mn)	0.15
8	Phosphorus (P)	0.01
9	Sulphur (S)	0.002
10	Titanium (Ti)	0.1

Table3: Elemental analysis obtained of the silicon (mgSi) used for fabricating FeSi samples.

Sr no.	Element (symbol)	Content [wt. %]
1	Aluminium (Al)	0.25
2	Calcium (Ca)	0.03
3	Copper (Cu)	0.018
4	Iron (Fe)	0.3
5	Phosphorus (P)	0.051
6	Titanium (Ti)	0.055
7	Silicon (Si)	99.3

Table4: Elemental analysis of the recycled silicon (reSi) used for fabricating FeSi samples.

Sr no.	Element (symbol)	Content [wt. %]
1	Aluminium (Al)	0.64
2	Boron (B)	0.01
3	Copper (Cu)	0.053
4	Lead (Pb)	0.05
5	Phosphorus (P)	0.03
6	Cadmium (Cd)	0.05
7	Silver (Ag)	0.192
8	Tin (Sn)	0.014
7	Silicon (Si)	98.96

Table 5: Experiment plan to prepare 250g of FeSi10, FeSi20 and FeSi45 from three different sources of Si.

Total sample weight [g]	Si content in FeSi [%]	Fe [g]	mgSi [g]	FeSi75 [g]	reSi [g]
250.5		225	25.5	X	X
252.0	10	217	X	35	X
251.0		225	X	X	26
251.0		200	51	X	X
253.0	20	183	X	70	X
252.0		200	X	X	52
252.0		138	114	X	X
256.0	45	99	X	157	X
254.0		138	X	X	116

2.2 Preparation of samples in the furnace.

The amount of iron required for the sample was measured and placed in the alumina crucible. The alumina crucible was placed inside a larger graphite crucible. The dimensions of both crucibles along with the weights are given in the table 6. To remove the volatiles from the crucibles, all crucibles were annealed at 1000C for 10 minutes in normal air. The graphite crucible lost ≈210 g after the annealed, while there was no appreciable change in the weight of the alumina crucible.

Table 6: Dimensions and weight of the graphite and alumina crucibles used in the experiments.

Crucible type	Height [mm]	Inner Diameter [mm]	Thickness [mm]	Weight as received [g]	Weight after baking [g]

Graphite	100	55	25	1082±3	871±1.3
Alumina	80	48	2.5	120±1.5	119±0.2

Before the sample preparation, the amount of Si sources required for each experiment were dried in in a hot air oven at a temperature of 120 C for 30 minutes. Then they were crushed using mortar and pestle and then were passed through sieve to obtain silicon feed material with particles less than 2mm in size. To prepare the sample, the required amount of iron was weighed and placed inside the alumina crucible. The crucibles were placed inside the induction furnace and covered with an alumina lid with an opening in the centre through which a thermocouple was inserted to record the temperature. After the iron melted, the temperature of the molten iron was ascertained before addition of Si source, and then the measured amount of the appropriate silicon source (according to the experiment design) was added to the crucible. The contents were stirred (intermittently) with the help of a clean quartz tube to check for complete dissolution. After the complete dissolution of the Si in Fe, the first sample was collected using a quartz tube of diameter 1.8 mm using suction process. The sample withdrawn using quartz tube ranged from 7-10 g. This sample was allowed to cool down to ambient temperature naturally, after which the sample was recovered by breaking the quartz tube. After retrieving the first sample, the furnace was turned off. The remaining mass of the sample was left in the crucible which was covered with the alumina lid (with an opening in the centre) the sample was allowed to cool down naturally to room temperature. After the sample and the crucible had cooled down, the alumina crucible was broken to retrieve the sample. The sample retrieved using quartz tube took 20-30 minutes to cool down to ambient temperature while that in the furnace took 150-200 minutes to cool down to ambient temperature. For each type of sample, the experiment was repeated three times, leading to three samples for each sample type.

Some samples were prepared in a plasma arc furnace in argon atmosphere to compare the impact of processing conditions on the sample. To prepare such samples, the calculated and measured amount of raw materials (Fe + Si) were placed on the water-cooled copper worktable of the furnace. The furnace chamber was flushed with Argon thrice and the working pressure was set at 800 mbar. Samples prepared using arc furnace were cooled in air and it was not possible to carry a long cooling process. The samples from the arc furnace tool 15-20 minutes to cool to room temperature, during which the chamber was flushed with Argon and was kept pressurized, to prevent air leaking into the furnace chamber. Hence, for comparing the properties of the sample prepared in Arc furnace with those prepared in the induction furnace, only the samples collected from the latter using the quartz tube were considered.

The obtained FeSi samples were cut using a circular saw and mounted on cylindrical samples using thermosetting carbon resin. The samples were then polished using different grades of sandpaper, ranging from 100 to 4000. For sandpapers, the grades refer to the number of particles per mm^2 of the paper. Therefore, sandpaper of lower grade is coarse while that of higher grade is fine. The final polishing was done using an automatic polisher using alumina (≈1μm) as the abrasive. The samples were first washed in alcohol and then in DI water and then in alcohol again using an ultrasonic cleaning tub. The samples were dried using an IR lamp and then immediately taken for characterization.

2.3 Characterization of the samples

The microstructure of the samples was analysed using scanning electron microscope, while the chemical composition was ascertained using an integrated energy dispersive X-ray spectroscopy. The different phases in the samples were identified using X-ray diffraction. The hardness of the samples was also evaluated using a standard Vickers hardness tester using HV10 (test force of 10 kg).

2.4 Sample symbol and notations

A large number of samples with different sources of Si, different concentration of Si and different process routes were prepared and analysed in this work. To make the text easily understood and concise, each sample is provided with a notation to identify most of the processing parameters. The sample identification notation followed in this work is,

Z_XXSi_FeSiyy-k

Where,

Z - This character defines the furnace type used to prepare the sample. 'I' would represent induction furnace, while 'A' would represent the Arc furnace.

XXSi - These letters represent the source of Si used for fabricating the samples. Three sources are used which are assigned a letter each for their identification.

i. Commercially procured metallurgy grade silicon – 'mgSi'
ii. Commercially procured FeSi75 – 'FeSi75'
iii. Recycled silicon from electronic waste – reSi

yy – These represent the percentage of Si in the FeSi sample. In this work, we have produced samples with three different percentages of Si. Hence, the values of yy are 10, 20 and 45.

k – This symbol represents the cooling process of the samples. Samples that cooled down within 20-30 minutes in ambient air for induction furnace, or within 10 min in water cooled crucible in arc furnace, were referred to as quenching (q). On the other hand, the samples that were cooled inside induction furnace to ambient temperature, were referred to as annealed (a) samples.

2. Simulations of phases formed in FeSi using FactSage.

FactSage 8.3 was used to simulate the number and the amount of components formed at different percentages of silicon. All calculations using FactSage represent the equilibrium cooling conditions. However, equilibrium cooling conditions could not be maintained during the solidification and cooling of the sample. Therefore, the results presented here are theoretical approximations of the system and are used as a guideline for identification of the different phases present in the actual sample. In the following sections we present a succinct overview of the phase transition temperatures and the accompanying phases. The Fe-Si binary phase diagram for silicon wt. fraction between 0.05 to 50% is shown in figure 1.

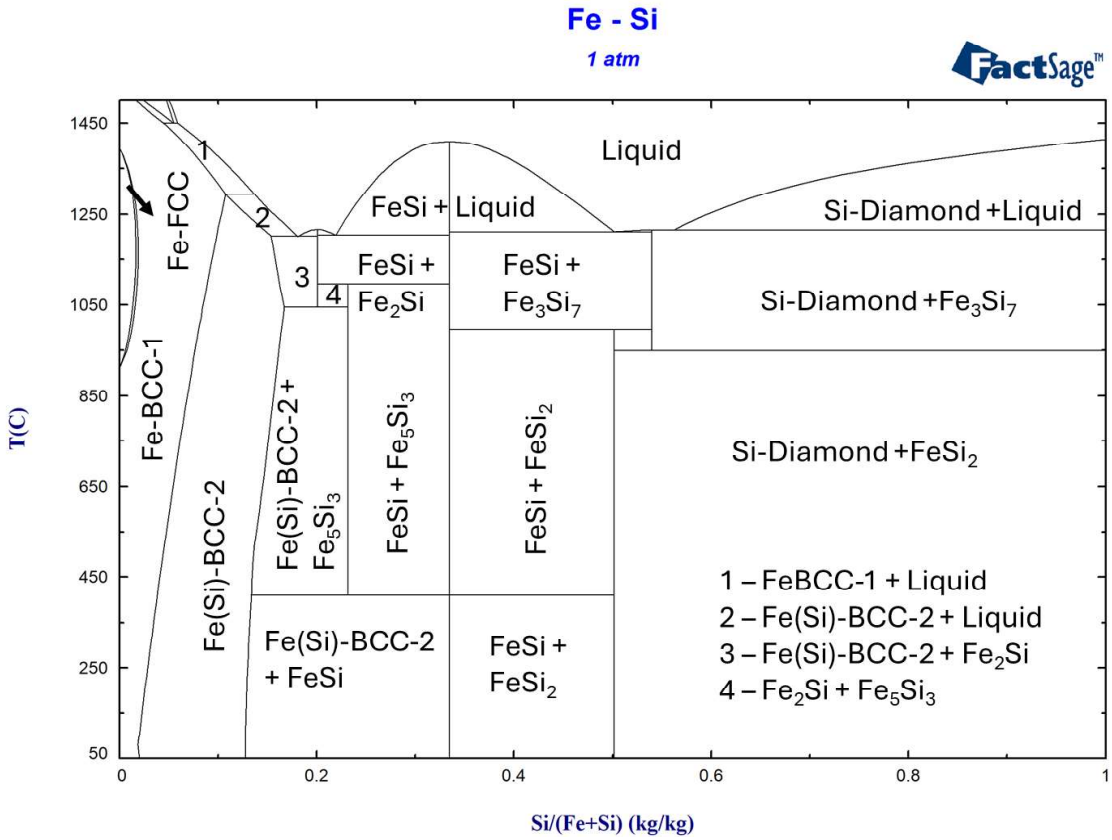

Fig 1 – Fe-Si binary phase system as reproduced with the help of FactSage 8.3.

FESi10- FeSi10 begins to solidify at 1315 ℃ into BCC FeSi solid solution. The alloys remain as a stable solid solution until 1200 when a solid-state transition takes place. The single solid solution of FeSi forms two solid solutions – a Fe rich solution which is in majority and a small portion of Si rich solution, both having BCC lattice. As the alloy is alloyed to cool under equilibrium, the silicon rich alloy gradually dissolves and the Fe and Si are absorbed by the Fe rich alloy, leaving only the Fe rich, BCC FeSi in the final state. The change in the mass of the Fe-rich and Si rich BCC components as the FeSi10 alloys cools down is shown in figure 2.

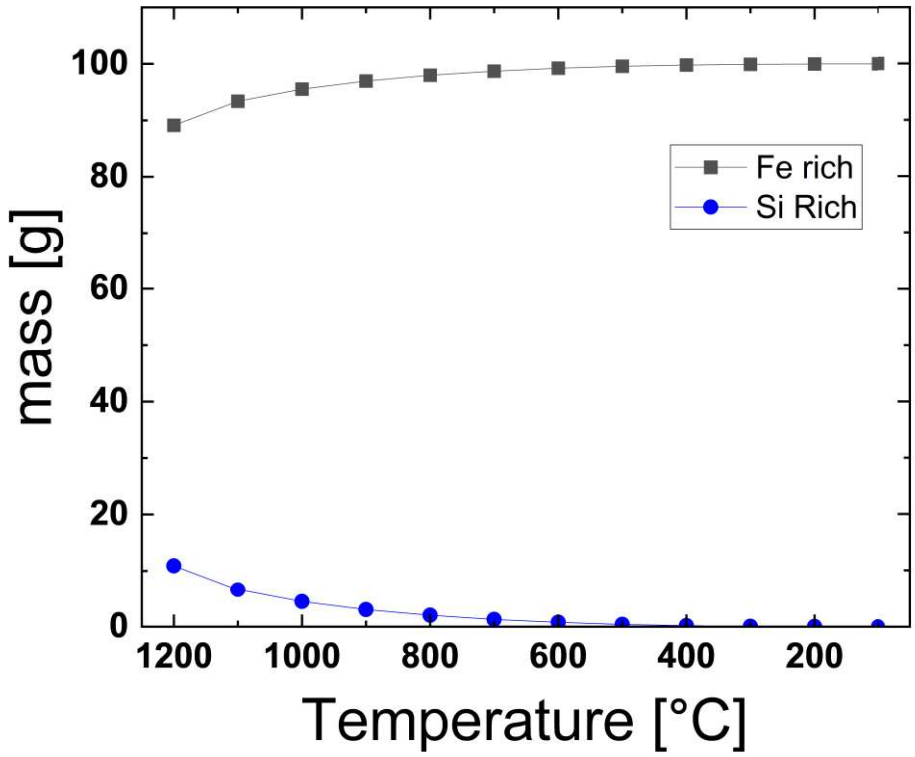

Fig 2: The change in the Fe rich and Si rich component of FeSi10 alloys while cooling down under equilibrium cooling conditions as predicted by FactSage.

FeSi20 – FESi20 remains in liquid state until 1200 ℃. The solidification of the of the alloy begins between 1215-1200 ℃, where an intermediate Fe_2Si appears. In this case, the entire liquid does not change into solid at once. The first solid state appears at 1215 ℃, and at 1200 ℃ ≈ 4.6g of the alloy exist in liquid state. At 1100 ℃, the alloy is completely solid and consists of small portion of Fe-rich and further smaller portion of Si rich BCC alloys, along with a major portion of Fe_2Si. At 1044.32 ℃, the entire amount of Fe_2Si undergoes a solid phase transformation, with a portion of it appearing as Fe_5Si_3 while the remaining portion contributing to the increased amount of Fe-rich and Si-rich BCC solid solutions. As the alloy continues to cool down, the amount of Fe_5Si_3 increases with a corresponding decrease in the Fe-rich and Si-rich BCC alloys. Finally at 409.1 ℃, the solid Fe_5Si_3 undergoes solid state transformation under equilibrium conditions. A portion of Fe5Si3 gets converted to FeSi, while the remaining portion add to the Fe-rich BCC alloy component. As the alloy cools down, the concentrations of Fe-rich and the Si-rich BCC alloys change slightly with a corresponding increase in the amount of FeSi. The change in the mass of the different alloy components with the cooling of the FeSi20 alloy is shown in figure 3.

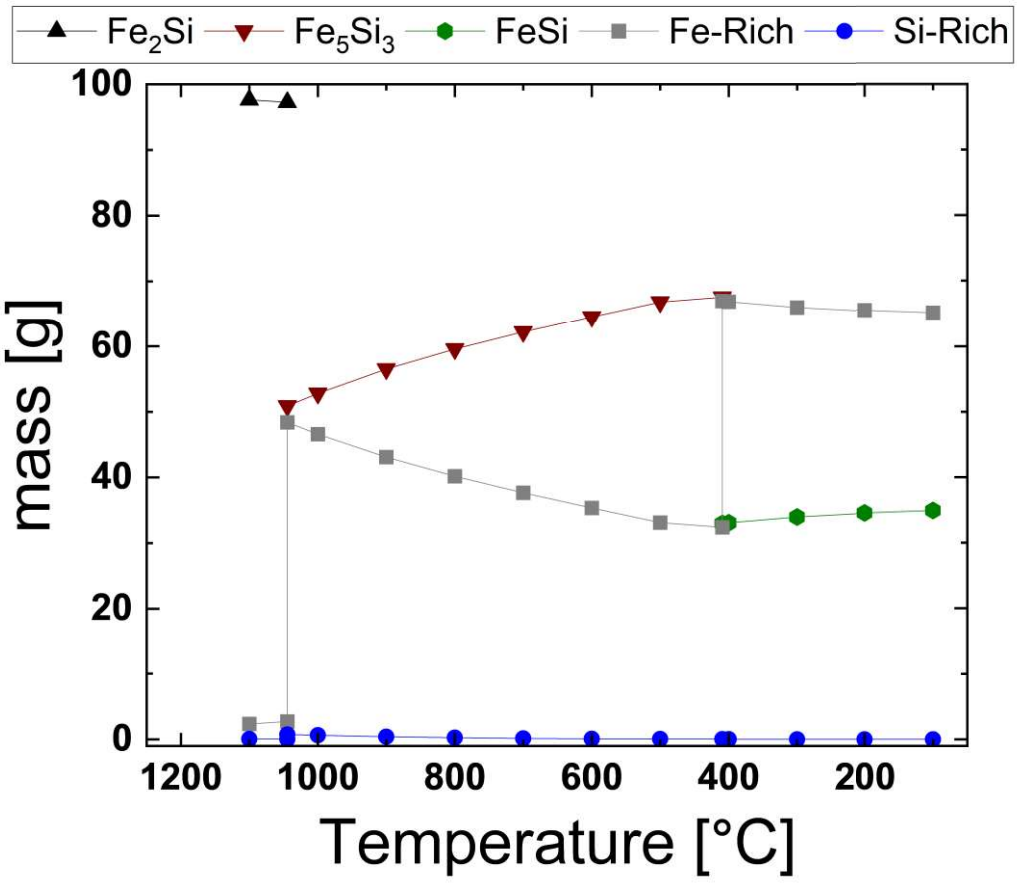

Fig 3: The change in the different components of FeSi20 alloys while cooling down under equilibrium cooling conditions as predicted by FactSage.

FeSi45: For FeSi454, the solidification begins ≈ 1210 °C, similar to FeSi-20. However, FeSi is the first solid phase to appear in FeSi45, which is immediately followed by appearance of Fe_3Si_7. The BCC phase prevalent in both FeSi10 and FeSi20 does not appear here and the quantity of both FeSi and Fe_3Si_7 remains stable as the alloy cools. At ≈995.8 °C, entire Fe_3Si_7 transforms to $FeSi_2$, consequently reducing the amount of FeSi. Beyond this temperature no further phase changes occur and the amount of FeSi and $FeSi_2$ remains stable as the alloy cools down to 100 °C. Figure xx show the appearance and the amount of different component of the phases as the FeSi45 alloy cools down under equilibrium. Figure 4 shows the change in the amount of different components of the alloy system with temperature as calculated using FactSage 8.3 in equilibrium cooling conditions.

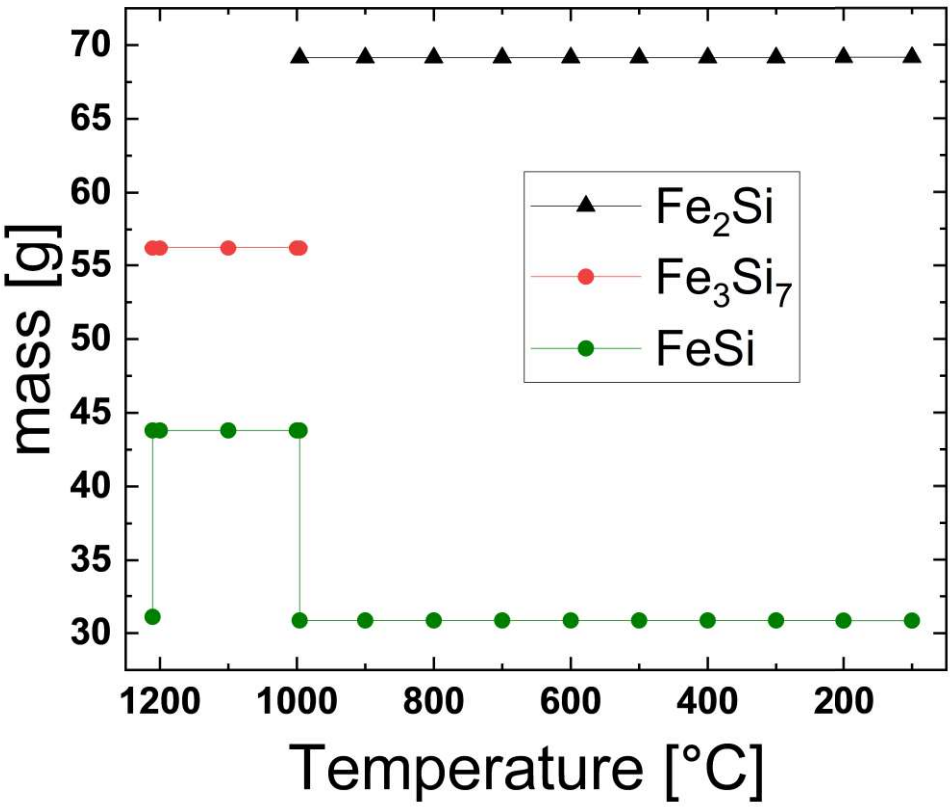

Fig 4: The change in the different components of FeSi45 alloys while cooling down under equilibrium cooling conditions as predicted by FactSage.

3. Results and discussion

3.1. Effect of silicon concentration (wt.%) and the source of Si on the properties of FeSi prepared using Induction furnace.

3.1.1. Mass balance for the samples prepared.

Tables 7 shows the mass balance of FeSi10, FeSi20 and FeSi45 prepared from different Si sources. It was observed that the material loss, both in absolute weight and as a percentage of the total weight of the sample, was least for the recycled silicon. The maximum material loss was observed when commercial mgSi was used as the silicon source, followed by FeSi75 as silicon source. The trend remained unchanged despite the change in the fraction of Si in the FeSi. Furthermore, the material loss increased with the increasing fraction of Si in the FeSi samples. While for I_mgSi_FeSi10, 0.64% wt. of the original mass of the sample was lost, for I_mgSi_FeSi45 this percentage rose to almost 3%. The material loss was also found to be almost directly proportional to the mass of Si source used in preparing the sample. For example, from table 7 it can be seen, that the material lost for all FeSi10 samples is roughly half of that lost in all FeSi20 samples, which is again roughly half of that lost in all FeSi45 samples. It can be inferred from this observation that the silicon source was mostly responsible for the material loss. Material loss manifested as a thin layer of material stuck to the alumina crucible and in the form of tiny, oxygenated granules which were removed from the surface of the sample before measurement. Some material also stuck to the stirrer and the quartz tube used for

retrieving the sample, which were lost and could not be recovered. It was observed that with increasing fraction of Si, the later attached to the Al crucible became thicker, mostly at the bottom of the crucible. On observing the broken crucible under SEM, it was observed that the layer of material attached to the bottom of Al crucible was between 200-400 μm thick for I_mgSi_FeSi10, while it was ≈ 900μm thick (at the centre of the crucible) for I_mgSi_FeSi45. These observations could be explained based on the time taken for melting of Si and its dissolution in the Fe. As the fraction of Si in the FeSi increases, the fraction of Fe decreases. This reduces the speed of dissolution of Si in Fe and could provide more time for the Si to react with the Alumina crucible where it could form a thin layer of Aluminosilicates, or for the Si to be oxidized leading to formation of oxides. FeSi75 usually melts in the temperature range of 1250-1350 ℃, while pure silicon melts at 1400℃. Hence, the mgSi and reSi would need more time to dissolve than the FeSi75. However, the reSi (monocrystalline silicon from PV panels) melted and dissolved quicker than the mg-Si. While the exact reason for this could not be established for certain, it could be attributed to the dimensions of the Si chips obtained from the EOL PV panels. The thickness of the solar cells used in the commercial PV panels is usually in the range of 110-150 μm [36]. This corroborates with our observation while preparing FeSi45 samples, where reSi dissolved quicker than the mg-Si samples for the different FeSi samples. Further, the percentage of volatiles in reSi is expected to be minimum as high-quality silicon is used for manufacturing solar cells [37]. Visually, least fumes were observed during addition of reSi and later least amount of oxides and debris were found in the FeSi samples prepared with reSi. Hence, all these observations point towards reSi being a good Si source for preparation of FeSi.

Table 7: Mass balance for samples prepared in an open induction furnace with different wt.% of silicon using different sources of silicon. The total wight of sample is the sum of both quenched and annealed samples. The data presented is the average of three observations.

Sample ID	Si source type	% wt. of Si [%]	Fe wt. [g]	Si source wt. (s) [g]	Total in (a) [g]	Total weight of sample [g]	Material loss (l) [g]	l/a [%]
I_mgSi_FeSi10	mgSi	10	225.2	25.6	250.8	249.2	1.6	0.64
I_ FeSi75_FeSi10	FeSi75	10	217.3	35.1	252.4	251.1	1.3	0.52
I_reSi_FeSi10	reSi	10	225.1	26.1	251.2	250.5	0.7	0.28
I_mgSi_FeSi20	mgSi	20	200.3	51.3	251.6	248.5	3.1	1.23
I_ FeSi75_FeSi20	FeSi75	20	183.5	70.4	253.9	251.1	2.8	1.10
I_reSi_FeSi20	reSi	20	200.2	52.1	252.3	250.8	1.5	0.59
I_mgSi_FeSi45	mgSi	45	138.1	114.2	252.3	244.8	7.5	2.97
I_FeSi75_FeSi45	FeSi75	45	99.2	157.1	256.2	250.6	5.6	2.18
I_reSi_FeSi45	reSi	45	138.2	116.1	254.2	250.9	3.3	1.29

4.1.2 Microstructure and Si content of the FeSi samples prepared with different Si sources.

The microstructure of the samples was analysed using SEM. The chemical composition of the samples was also analysed for the final Si content using EDS measurements. The observed area was divided into a grid of 5 smaller areas and EDS measurements of these individual smaller areas were taken. The process was repeated for all the three samples for each type of sample prepared, resulting in a total of 15 observations. Finally, the results were averaged. This was done to identify any preferential segregation of the Si or formation of any intermetallic compounds.

Figure 5 shows the micrographs of the cross section of the FeSi10-a samples prepared using different sources of Si, while figure 6 shows the cross section of FeSi10-q samples. Since the Si content is low, the microstructure still corresponded to steel's microstructure and different grains of steel could be observed in the backscattered electron image. The silicon was evenly distributed throughout the microstructure and minimum inhomogeneity was observed. In the I_reSi_FeSi10-a samples, particles of Ag thoroughly distributed throughout the microstructure were observed. This is not surprising as Ag is known to have low solid solubility in both Fe and Si.[38,39]. The microstructure of the samples quenched in air was similar in nature, except for the grain size which were smaller than those in the annealed samples.

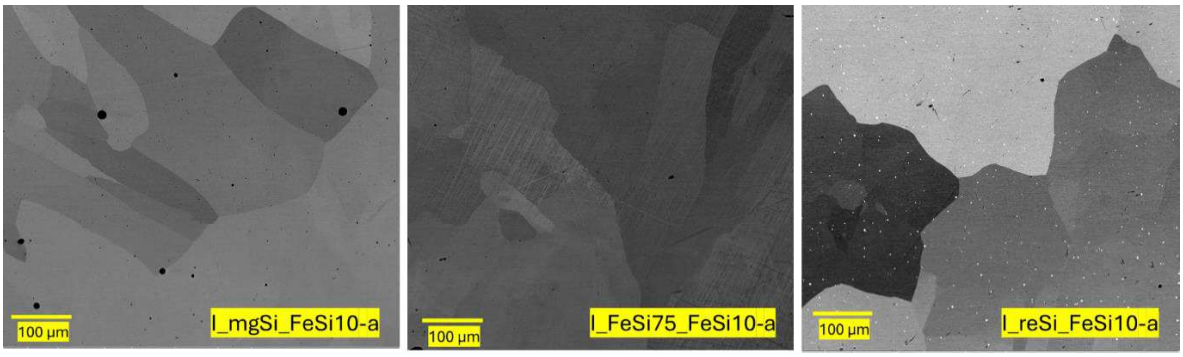

Figure 5: SEM micrographs of the cross section of the FeSi10 prepared using different sources of Si. All the samples shown here were allowed to cool in the furnace.

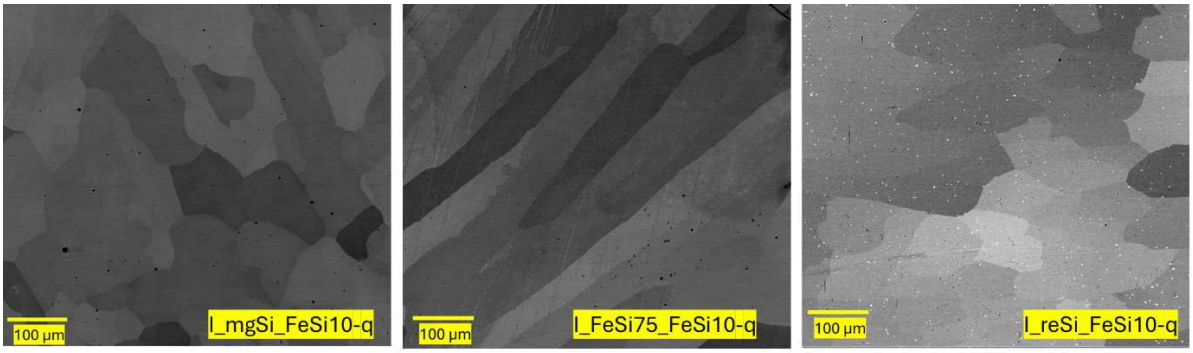

Figure 6: SEM micrographs of the cross section of the FeSi10 prepared using different sources of Si. All the samples shown here were obtained using quartz tube and cooled rapidly in air.

The Si concentrations in the FeSi10 alloys prepared is shown in Table 8. Based on averaged EDS measurements from 15 points, the weight content of Fe and Si varied for different sources of Si. In the case of FeSi10, samples with the highest content of Si were obtained with metallurgical grade Si as the source of Si. The differences between Si content were minor and was recorded maximum to be ≈ 0,6% wt. abs. between the highest (mg Si) and the lowest content (commercial FeSi75). In the case of additional elements (originating from input materials) in the alloys. FeSi obtained from FeSi75 had the highest content of ≈1.6 %, and the lowest content was noted for metallurgical grade Si (≈1.4%). The difference in the percentage of Si in FeSi10 samples prepared from mgSi and reSi as Si source was negligible. Furthermore, the difference in the chemical composition and distribution of Si between the quenched and annealed samples was also negligible. The other elements comprised predominantly Al, Ca, Cu, Mg and, in case of samples prepared with reSi , Ag. While the presence of other impurities, including carbon cannot be ruled out, their concentration could not be confidently determined using EDS as they were below the detection limit of the equipment.

Table 8. Averaged chemical content of I_FeSi10 alloys based on SEM, EDS.

Sample ID	Fe content [wt.%]	Si content [wt.%]	Other elements [wt.%]
I_mgSi_FeSi10-a	89.6±0.2	8.8±0.2	1.4±0.1
I_ FeSi75_FeSi10-a	89.1±0.5	8.2±0.3	1.6±0.4
I_reSi_FeSi10-a	89.5±0.2	8.7±0.3	1.5±0.2

Figure 7 shows the micrographs of the cross section of the FeSi20-a samples prepared using different sources of Si, while figure 8 shows the micrographs of the cross section of FeSi20-q samples. In these images, the segregation of Si rich parts could easily be seen. In all the SEM images, the lighter regions correspond to the Si rich region while the darker regions correspond to Fe rich regions. The distribution of Si-rich regions was found to be visually similar in annealed and quenched samples prepared using different silicon sources. However, upon further analysis of the images using ImageJ, minor differences were observed between the annealed and the quenched sample. The area fraction of the Fe rich regions (dark shaded) was found to be 5-7% less than that in the annealed samples. Hence, the samples which took longer to cool down had higher fraction of FeSi20 and lower fraction of Fe rich regions. In FeSi20 samples prepared using mgSi Al could be seen along the grain boundaries. In the FeSi20 samples prepared using reSi, circular clusters of Ag could be seen randomly distributed, mostly at the grain edges or boundaries. Further, the clusters were larger (3-7 μm) but less in number in the annealed samples, while those observed in the quenched samples were smaller (1-4μm) but more in number. The slower cooling rate in the case of annelid samples allowed for the diffusion, agglomeration and growth of Ag clusters, which were easily identified. The Al segregated along the grain boundaries only in I_mgSi_FeSi20 samples. Similar behaviour was not observed in the I_reSi_FeSi20 samples, while the proportion of Al in both mgSi and reSi was similar (Tables 2 and 4). While the exact reason for this is not known, we suspect that this

is due to the presence of Ag in the latter samples. It was noted that the circular (spheroidal) globules formed were predominantly Ag alloys, than only Ag or Al. This can be attributed to the rather good solid solubility of Ag in Al [40,41]. Further, in solar cells, both Ag, Al and alloys of Ag and Al are present in the meal paste for forming the electrical contacts, along with some other elements such as lead (Pb), cadmium (Cd) and tin (Sn) [42–44].

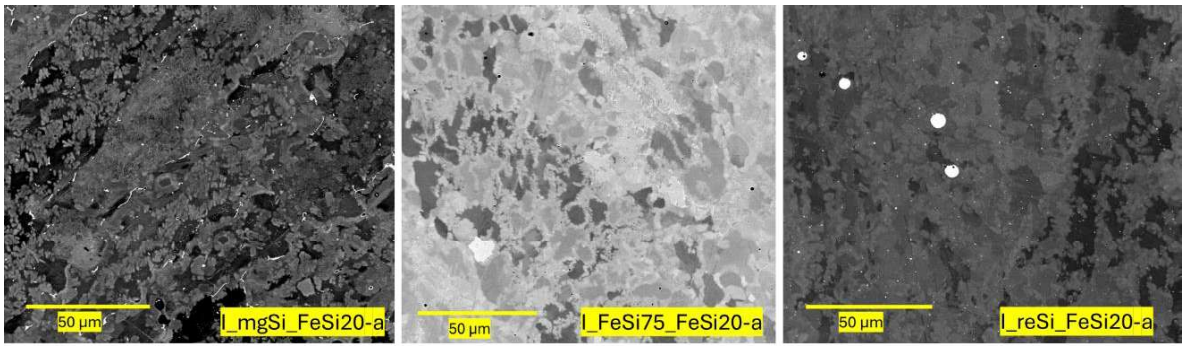

Figure 7: SEM micrographs of the cross section of the I_FeSi20-a prepared using different sources of Si. All the samples shown here were allowed to cool in the furnace.

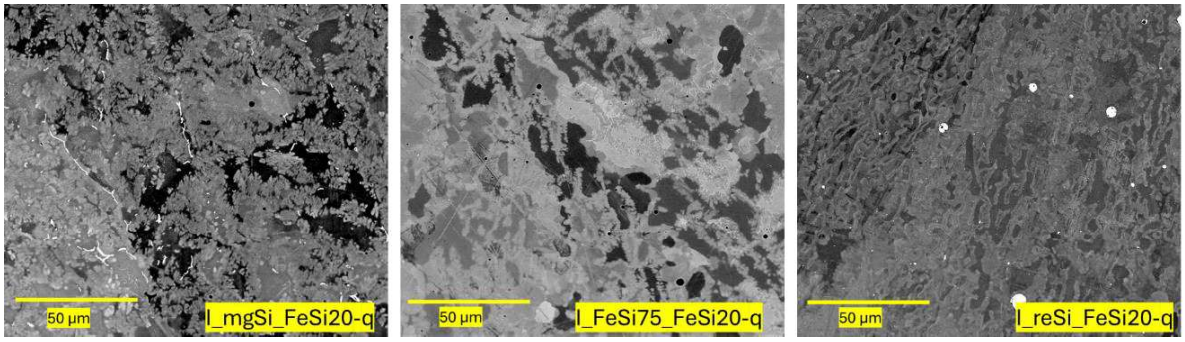

Figure 8: SEM micrographs of the cross section of the I_FeSi20-q prepared using different sources of Si. All the samples shown here were obtained using quartz tube and cooled rapidly in air.

The samples were further analysed using EDS to characterize their chemical composition. The Fe rich regions visible as darker regions in the SEM images (Figures 7 and 8) were more than 90% Fe, and this characteristic was similar in all the samples irrespective of the cooling time or the type of Si source used. Therefore, for further comparison of the samples, only the FeSi regions were analysed. Table 9 and table 10 show the composition of the FeSi regions in the annealed and quenched I_FeSi20 samples respectively. The FeSi regions were selected to exclude the precipitated Al dendrites and Ag globules. While there were minor differences in the composition of FeSi in the quenched and the annealed samples, there was a larger variation in the uniformity of the distribution between the quenched and the annealed samples. As the annealed samples slowly cooled down in the residual heat of the furnace, they had more time for homogenization and hence resulted in improved uniformity in the composition of FeSi20. In the case of I_FeSi20 samples, like the I_FeSi10 samples prepared with mgSi as Si source resulted in the highest percentage of Si in the FeSi. Samples prepared with reSi silicon had slightly lower concentration of Si, followed by those prepared with FeSi75 where the Si content

was least. Like the FeSi10 samples, the concentration of Si was lower that the targeted value (20% wt.) by 1.3-2.5% wt.

Table 9: Averaged chemical content of I_FeSi20-a alloys (FeSi regions only) based on EDS. The data presented here is the average of 5 points per sample, across three samples (total 15 points)

Sample ID	Fe content [wt.%]	Si content [wt.%]	Other elements [wt.%]
I_mgSi_FeSi20-a	80.1±0.5	18.7±0.3	1.2±0.2
I_ FeSi75_FeSi20-a	79.8±0.9	17.5±0.5	2.7±0.5
I_reSi_FeSi20-a	79.9±0.4	18.5±0.4	1.6±0.3

Table 10: Averaged chemical content of I_FeSi20-q alloys based on EDS. The data presented here is the average of 5 points per sample, across three samples (total 15 points)

Sample ID	Fe content [wt.%]	Si content [wt.%]	Other elements [wt.%]
I_mgSi_FeSi20-q	81.4±2.5	17.5±2.3	1.1±0.3
I_ FeSi75_FeSi20-q	80.6±2.9	16.9±2.5	2.5±0.5
I_reSi_FeSi20-q	80.3±2.4	17.9±2.5	1.8±0.4

The compositions of Al segregated along the grain boundaries in the I_mgSi_FeSi20-a and the Ag crystallites in the I_reSi_FeSi20-a were also analysed using EDS. The Al segregated along the boundaries in I_mgSi_FeSi20 samples included Al, Cu, Ca and Ti, where Al and Cu together contributed more than 90% of the composition by mass. On the other hand, in the Ag crystallites in the I_reSi_FeSi20-a samples were predominantly Ag (≈90% wt.) with small amounts of Al, Sn, Cd and Pb. While small amounts of Al were also found in some areas alloyed with FeSi, most of the Ag was assumed to be precipitated out of the FeSi solution, as Ag could not be detected in other regions. Ag, Pb, CD and Sn were always detected together in the crystallites, as they are commonly used in metal pastes for forming electrical contacts. However, EDS has its detection limit, and it is possible that some extremely small quantities of these elements could be dissolved in the FeSi regions.

Figures 9 and 10 show the cross-section SEM images of the I_FeSi45-a and I_FeSi45-q samples prepared from different source of silicon, respectively. In this case we see two prominent phases present in all the samples, irrespective of the source of Si used or the cooling process. As expected, the grains in the quenched samples are smaller than those in the annealed samples. The matrix, represented by the darker shade has almost equal proportions of Fe and Si. Fe rich islands are uniformly distributed throughout the matrix. In the I__reSi_FeSi45 samples, particles of Ag (alloyed with Al, Pb, Sn and Cd) were observed along the boundaries of the islands, in both quenched and annealed samples. In annealed samples, the Ag particles were larger in size (2-5μm) and less in number, while in the quenched samples they were smaller in size (<2 μm) but numerous. This observation was similar to the I_reSi_FeSi20 samples. A major difference observed in the I_mgSi_FeSi45 samples as compared to I_mgSi_FeSi20, was the absence of the Al precipitation along the grain boundaries. In the I_mgSi_FeSi45 samples, the Al was found to be distributed uniformly in the Fe rich islands

and in the matrix. To differentiate the two phases, and for easy understanding we refer the phase where Fe and Si are almost equal as the Si rich and other as Fe rich phase.

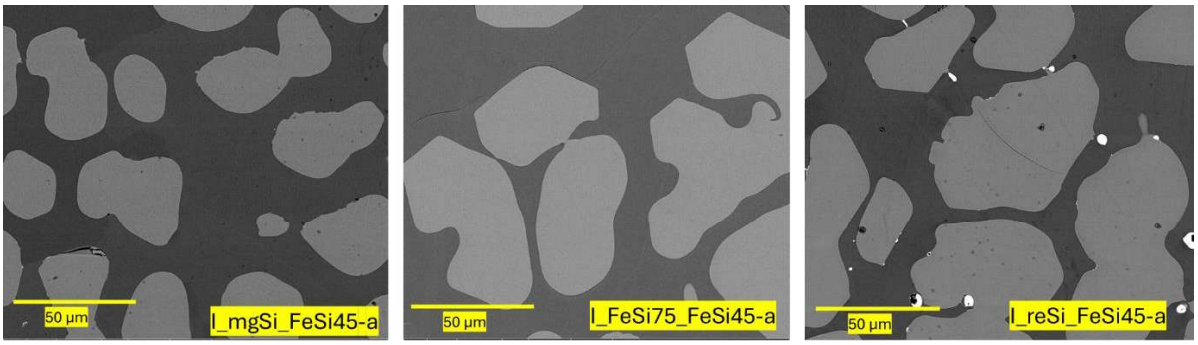

Figure 9: SEM micrographs of the cross section of the I_FeSi45-a prepared using different sources of Si. All the samples shown here were allowed to cool in the furnace.

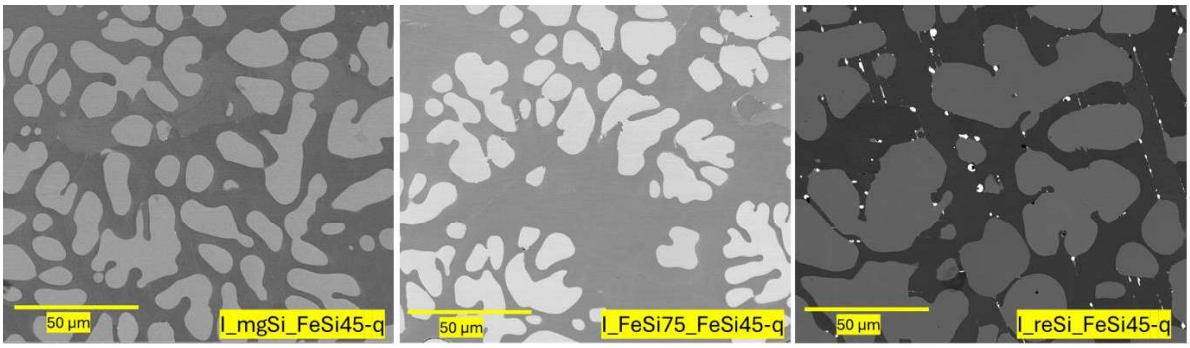

Figure 10: SEM micrographs of the cross section of the I_FeSi45-q prepared using different sources of Si. All the samples shown here were obtained using quartz tube and cooled rapidly in air.

Figure 11 shows the EDS map of a magnified portion of the I_reSi_FeSi45-a sample. The map was taken on a magnified image to obtain a good resolution for the Ag crystallites distributed throughout the microstructure. In figure 11, the difference in the Si content is clearly visible. The Ag crystallites can be observed located primarily along the boundaries of the grains having lower Si content. Cd was observed associated with Ag crystals, which as mentioned earlier, is included in the metal paste formulation used in the fabrication of solar cells. Al was found distributed throughout the microstructure quite uniformly in both Si rich and Fe rich regions. Other elements such as Pb and Sn were not clearly visible in the map, although they were identified and quantified. Tables 11 and 12 show the distribution of Fe and Si in the microstructure, both in the Fe rich and the Si rich phases, for the annealed and the quenched samples respectively. We observed that the Si rich regions in the annealed samples were closer to the desired composition of 45% wt. Si and 55% wt. Fe, than in the quenched samples. Hence, we believe that homogenization occurred during the extended cooling period in the annealed samples. However, it is noteworthy, that this extended time period was not enough to achieve complete homogenization. Nevertheless, presence of these two phases is common in commercial FeSi samples and have been reported earlier for FeSi75 [45,46]. Furthermore, it was also observed that the variation in the composition was larger in the quenched samples

than in the annealed samples, which is expected since the cooling duration was small. However, even air cooled FeSi45 was able to achieve the composition quite similar to the annealed FeSi45 as can be seen from Table 11 and 12. Since, FeSi is an intermediate product and is later used for alloying or deoxidation purposes, FeSi cooled in air should have similar performance to the FeSi annealed in the furnace. From these results it is clear that recycled Si from PV panels can be used to produce commercial FeSi.

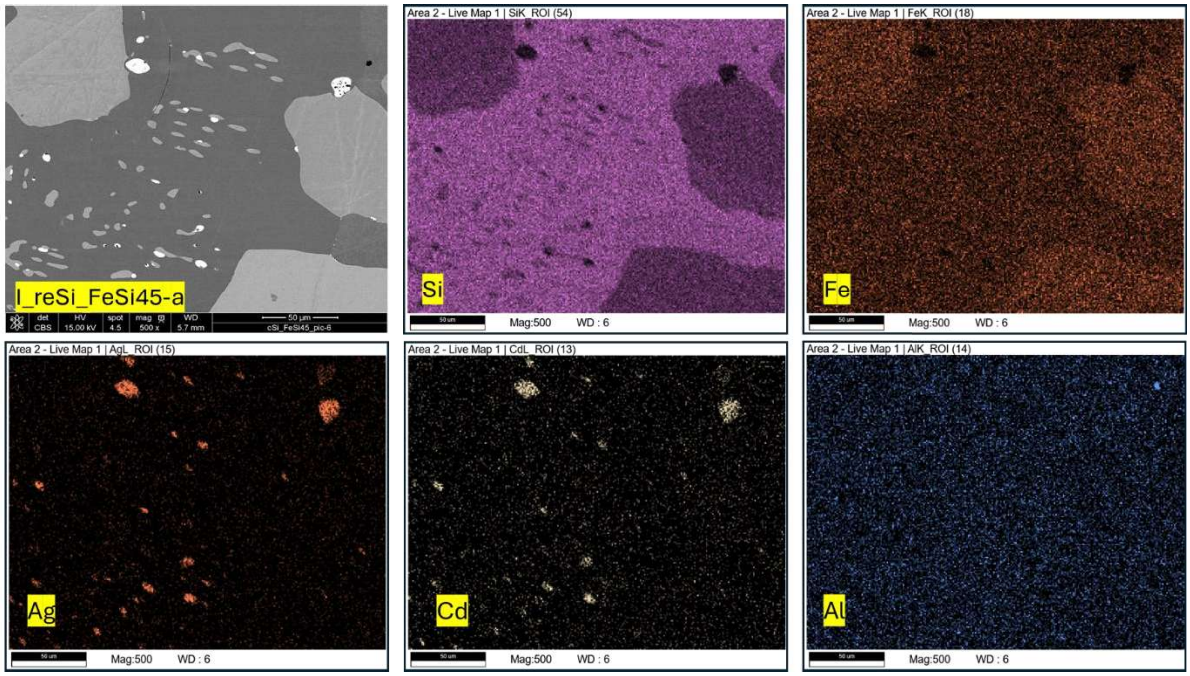

Figure 11: EDS map of I_reSi_FeSi45-a sample at 500x magnification showing the different elements identified.

Table 11: Averaged chemical content of I_FeSi45-a alloys based on EDS analysis. The data presented here is the average of 5 points per sample, across three samples (total 15 points)

Sample ID	Fe-rich			Si-rich		
	Fe content [wt.%]	Si content [wt.%]	Other elements [wt.%]	Fe content [wt.%]	Si content [wt.%]	Other elements [wt.%]
I_mgSi_FeSi45-a	67.1±1.8	32.2±0.5	0.7±0.3	51.4±1.7	47.9±0.2	0.7±0.3
I_ FeSi75_FeSi45-a	64.2±1.2	31.5±0.8	4.3±1.9	48.8±1.1	45.7±0.3	5.5±1.6
I_re_FeSi45-a	66.1±1.6	32.7±0.6	1.2±0.5	51.4±1.8	47.4±0.2	1.2±0.9

Table 12: Averaged chemical content of I_FeSi45-a alloys based on EDS analysis. The data presented here is the average of 5 points per sample, across three samples (total 15 points)

Sample ID	Fe-rich			Si-rich		
	Fe content [wt.%]	Si content [wt.%]	Other elements [wt.%]	Fe content [wt.%]	Si content [wt.%]	Other elements [wt.%]
I_mgSi_FeSi45-q	68.8±3.2	30.5±2.8	0.7±0.5	49.1±2.8	50.2±1.7	0.7±0.4
I_ FeSi75_FeSi45-q	64.5±3.8	30.7±2.9	4.8±1.1	44.9±3.2	50.2±1.8	4.9±1.7

I_re_FeSi45-q	68.0±3.1	30.8±2.8	1.2±0.6	48.5±2.2	50.3±1.4	1.2±0.9

4.2 Impact of the production process and atmosphere used for the formation of alloy on the properties of FeSi.

4.2.2 Mass balance for the samples prepared.

Table 13 shows the mass balance of the FeSi45 samples prepared in induction furnace and arc furnace under Argon atmosphere. The mass balance data of FeSi45 samples prepared in the induction furnace are copied from table 7 for easy comparison of data. Only FeSi45 samples were prepared in the arc furnace with different sources of Si. Since all the samples in the arc furnace were rapidly cooled in a water-cooled crucible hence, the quenched samples prepared in the induction furnace were used as reference samples for comparison of properties. The total loss in the sample is expressed as a percentage of the total mass of sample, as well as a percentage of the weight of Si source added to the sample. From table 13, it can be clearly seen that the material loss for samples prepared in Arc furnace is lower than those prepared in induction furnace for all samples. However, the overall material loss trend was similar in samples prepared in induction furnace and arc furnace. Samples prepared with reSi recorded lowest material loss while those prepared with commercial FeSi75 recorded the maximum loss, irrespective of the processing equipment or methodology. This data also suggests that presence of oxygen plays vital role in the material loss, probably due to the oxidation of the volatile impurities.

Table 13: Mass balance for FeSi45 samples prepared using different sources of silicon in an induction furnace and arc furnace under Argon atmosphere.

Sample ID	Si source type	% wt. of Si [%]	Fe wt.(f) [g]	Si source wt. (s) [g]	f/s	Total in (a) [g]	Total weight of sample [g]	Material loss (l) [g]	l/a [%]	l/s [%]
A_mgSi_FeSi45-q	mgSi	45	9.2	7.6	0.8	16.8	16.6	0.2	1.19	2.63
I_mgSi_FeSi45-q	mgSi	45	138.1	114.2	0.8	252.3	244.8	7.5	2.97	6.57
A_FeSi75_FeSi45-q	FeSi75	45	4.2	6.6	1.5	10.8	10.6	0.2	1.85	3.03
I_FeSi75_FeSi45-q	FeSi75	45	99.2	157.1	1.5	256.3	250.6	5.6	2.18	3.56
A_reSi_FeSi45-q	reSi	45	11.4	9.5	0.8	20.9	20.8	0.1	0.47	1.05
I_reSi_FeSi45-q	reSi	45	138.2	116.1	0.8	254.3	250.9	3.3	1.29	2.84

4.2.2 Microstructure and Si content of the FeSi samples prepared with different furnaces.

Figure 12 shows the EDS map of a cross section of A_reSi_FeSi45-q and I_reSi_FeSi45-q samples. The microstructure for both samples appear to be similar with no visibly discernible

differences. The distribution of the Si, Fe and Ag also appear to be similar. The Si rich and Fe rich portions are clearly visible while the Ag crystallites are located primarily at the grain boundaries of the Fe rich portions.

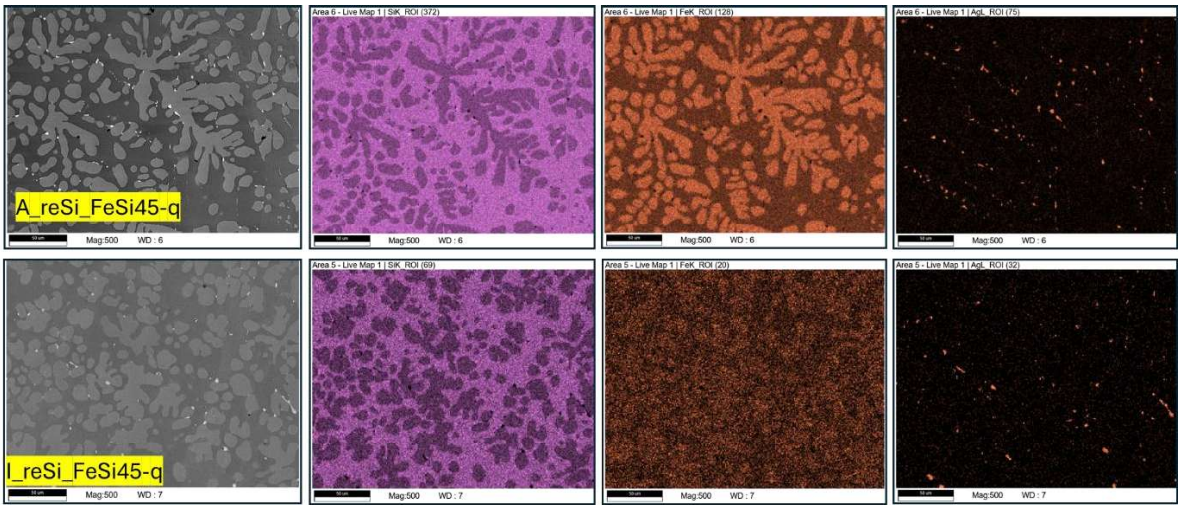

Figure 12: EDS maps of A_reSi_FeSi45-q and I_reSi_FeSi45-q samples at 500x magnification showing the different elements identified.

Table 14 shows the composition of Si and Fe in the Fe rich and Si rich phases in the FeSi45 samples prepared in Arc furnace using different sources of silicon. The data in table 14 can be compared against the data in table 12, which shows similar information for the samples prepared in arc furnace and cooled in air. It was seen that the impurities and other elements (besides Fe and Si) were higher in the samples prepared in arc furnace for the samples prepared with mgSi and reSi. However, the impurities content remained similar for the samples prepared with FeSi75. For example, in I_mgSi_FeSi45-q, other elements constituted only ≈ 0.7% wt. in the Fe and Si rich regions of the microstructure as determined by EDS. On the other hand, in A_mgSi_FeSi45-q, other elements constituted ≈ 3.1 % wt. and ≈3.8% wt. in the Fe rich and Si rich regions respectively. However, when this data is viewed along with the mass balance data, it is clear that most of the loss in the mass of the samples prepared in the induction furnace could be attributed to the oxidation of the impurities in the Si source used for preparing the samples. In the arc furnace, the impurities were not oxidized and hence were incorporated into the final sample. Furthermore, it was observed that the impurities content did not change appreciably for the FeSi45 samples prepared using FeSi75 as silicon source. Impurities comprised 4.9% wt. and 4.6% wt. respectively for the Fe rich and Si rich regions in the A_FeSi75_FeSi45-q samples, which was almost similar to the 4.8% wt. and 4.9% wt. recorded for the Fe rich and Si rich regions in I_FeSi75_FeSi45-q samples. This implies that the impurities in the FeSi75 could not be easily oxidized. It was further observed that the increase in the impurity content was at the expense of Fe content in both Si and Fe rich regions for FeSi45 samples prepared with mgSi and reSi. This could mean that the impurities are associated preferentially with Fe than with Si.

Table 14: Averaged chemical content of A_FeSi45-a alloys based on EDS analysis. The data presented here is the average of 5 points per sample, across three samples (total 15 points)

Sample ID	Fe-rich			Si-rich		
	Fe content [wt.%]	Si content [wt.%]	Other elements [wt.%]	Fe content [wt.%]	Si content [wt.%]	Other elements [wt.%]
A_mgSi_FeSi45	66.9±0.4	30.0±0.2	3.1±0.6	46.2±0.4	50.1±0.2	3.8±0.5
A_ FeSi75_FeSi45	65.2±0.2	29.9±0.2	4.9±0.4	46.1±0.6	49.3±1.0	4.6±1.5
A_reSi_FeSi45	66.8±0.7	30.0±0.5	3.3±1.1	46.1±0.3	50.0±0.2	3.9±0.5

While the microstructure towards the centre of the cross section of the samples prepared in arc furnace and induction furnaces were similar, slight differences in the microstructure were observed at the edges of the samples prepared in arc and induction furnaces, owing to the difference in the cooling rates. Figure 13 shows the SEM images of microstructure at the outer edge of the FeSi45 samples prepared in arc and induction furnaces. The samples prepared in the arc furnace were solidified in a water-cooled brass tube while the samples prepared in the induction furnace were cooled in ambient air in a quartz tube. Hence, their cooling rate of both samples was slightly different. The impact of difference in the cooling rate was visible on the grain size and grain distribution in the microstructure. For both samples, directional growth of elongated could be observed closer to the edges, where the cooling rate is expected to be maximum. In the samples prepared in induction furnace, the elongated grains gradually change shape and size and lead to the randomly oriented grains. Similar observation could be made in the samples prepared in arc furnace and casted in water cooled tube, however, the transition from the elongated grains to the randomly oriented grains could be distinctly observed within a circular annulus running along the edge of the sample.

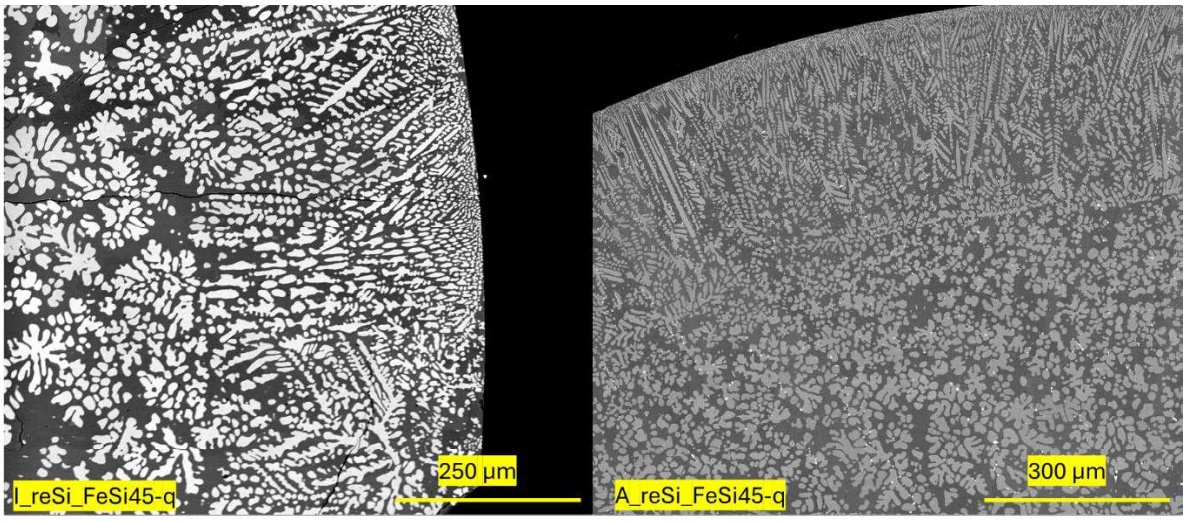

Figure 13: SEM images of the microstructure of the cross section of the samples prepared in induction and arc furnaces. The samples prepared in arc furnace were water cooled while those prepared in induction furnace were air cooled.

The samples prepared in arc furnace also exhibited cracks throughout the microstructure of the samples in the Si rich regions. Figure 14 shows the microstructure of the samples prepared in arc induction furnaces (quenched in air). Cracks were observed in the Si rich region of the microstructure in the samples prepared in arc furnace using mgSi and FeSi75 as silicon source. Interestingly, such cracks were not as abundant in the samples prepared using reSi as the silicon source. While the exact cause of this count be determined, we believe it is due to the presence of higher amount of Al and Ag distributed uniformly throughout the Si rich region in the samples prepared using reSi. Further analysis of the microstructure reveals that the Ag crystallites in the A_reSi_Fesi45-q samples were more elongated and directional than those in the I_reSi_Fesi45-q samples. Hence, we hypothesized that the presence of Ag crystals in the Si rich region prevented the cracks. Cracks more mostly absent in the samples prepared in the induction furnace and quenched in air as shown in fig 14.

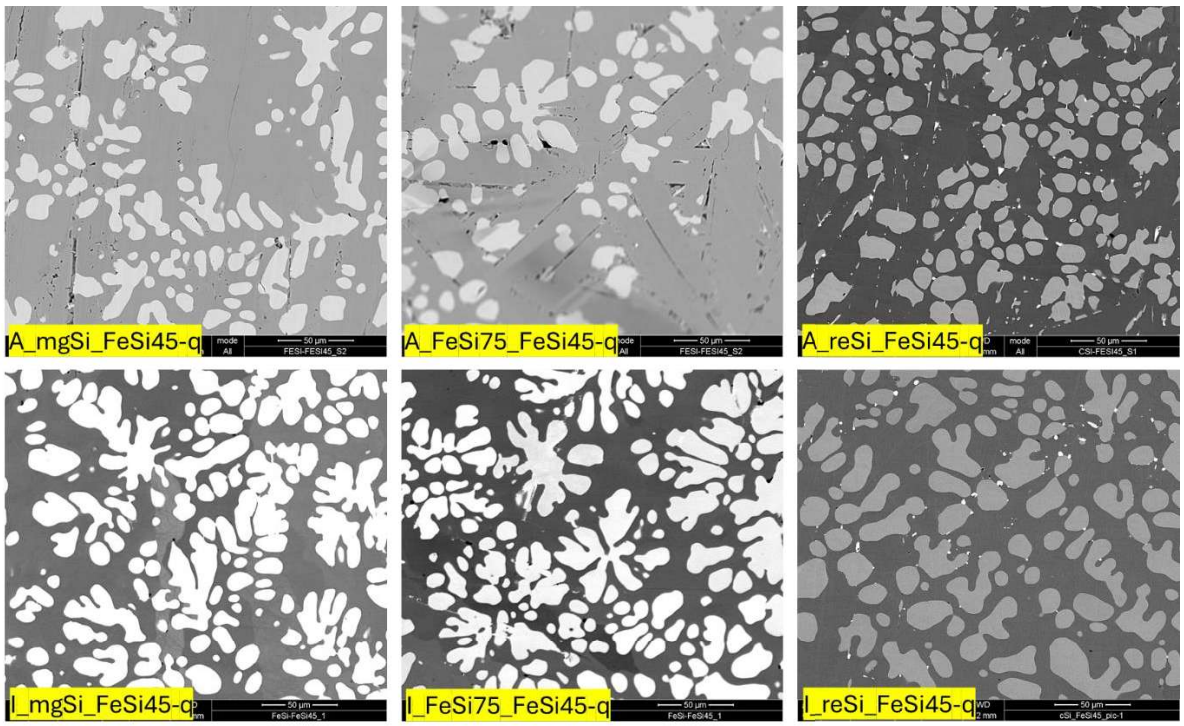

Figure 14: SEM micrographs showing the cross section of the FeSi45 samples prepared using different sources of Si in the arc and the induction furnaces. Cracks could easily be observed in the A_mgSi_Fesi45-q and A_FeSi75_Fesi45-q samples.

4.3 Analysis of the phases present in the samples using XRD

The samples were analysed using XRD to identify the phases present in the samples. Figure 15 shows the XRD analysis of FeSi samples with different percentages of Si prepared using reSi.

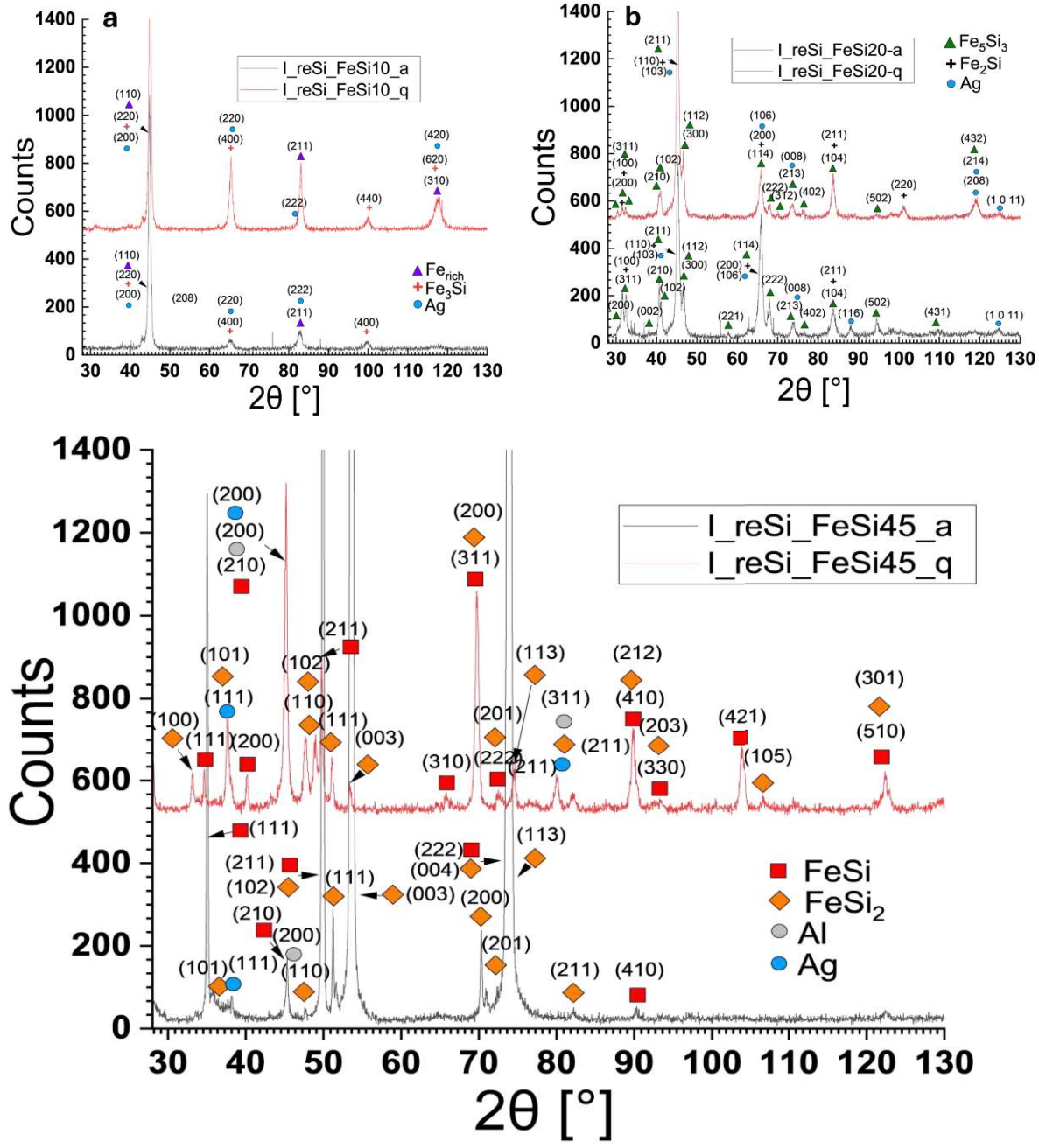

Figure 15: XRD patterns of FeSi samples with different percentages of Si prepared using reSi (a) I_reSi_FeSi10 (b) I_reSi_FeSi20 (c) I_reSi_FeSi45

The phases identified using XRD overall agreed with the theoretical simulations using FactSage. The longer cooling duration allows more time for phase transformation, hence higher fraction of stable phases is expected in the annealed samples. However, despite slow cooling, the cooling is not isothermal, hence, only a trend similar to the theoretical calculations is expected and a close agreement to the simulated data is not expected.

In I_reSi_FeSi10 samples, Fe_3Si (Cubic) and Fe (Cubic) phases are detected in both annealed and quenched samples. However, the fraction of Fe_3Si decreased in annealed samples (≈4%), while the fraction of Fe rich BCC solution increased in the annealed samples. In I_reSi_FeSi20

samples, Fe_5Si_3 (Hexagonal) and Fe_2Si (trigonal) phases were detected. In I_reSi_FeSi20-a samples, Fe_2Si and Fe_5Si_3 were present in the ratio 3:2, while in the I_reSi_FeSi20-q samples, Fe_2Si dominated (≈ 80%). The FeSi phase, which theoretically should appear at ≈ 410℃ for FeSi20, could not be detected in either sample, indicating slow kinetics for this transition. I_reSi_FeSi45 samples, FeSi (cubic) and $FeSi_2$ (orthorhombic) was detected in both quenched and annealed samples, as for FeSi45, FeSi phase theoretically appears at ≈1210 ℃. In I_reSi_FeSi45-a samples, the ratio of FeSi: $FeSi_2$ was ≈ 1:1.6 which is closer to the ≈1:2 ratio calculated using FactSage. In I_reSi_FeSi45-q samples, FeSi was dominant phase while $FeSi_2$ was present in smaller quantities, their ratio being ≈2:1. The Fe_3Si_7 phase, which is expected to exist only until 995℃ was not detected in both I_reSi_FeSi45 samples, indicating quick kinetics for the transformation from Fe_3Si_7 to FeSi and $FeSi_2$. While Ag was detected in all the samples prepared with reSi, however, Al could be identified only in FeSi45 (both quenched and annealed) samples. Same phases (FeSi, $FeSi_2$) were identified in XRD measurements done on I_mgSi_FeSi45 and I_FeSi75_FeSi45 samples. While Al was identified in both I_mgSi_FeSi45-a and I_mgSi_FeSi45-q samples, it was not detected in I_FeSi75_FeSi45 samples.

Figure 16 shows the XRD pattern of the FeSi45 samples prepared in arc furnace with different sources of Si. Phases similar to those detected in I_FeSi75 samples were also detected in the samples prepared with Arc furnace. The XRD pattens of the samples prepared in arc furnace resembled the quenched samples prepared with the induction furnace, which was expected. Ag and Al were detected only in the A_reSi_FeSi45-q samples and was not detected with high level of confidence in the other two samples. Slight differences were observed in the XRD patterns of individual samples. XRD patterns of A_reSi_FeSi45-q and A_FeSi75_FeSi45-q samples were more similar to each other, while that of A_mgSi_FeSi45-q was slightly different. This could be due to the slightly different fraction of the individual phases. The exact reason for the difference in the composition of phases could be determined, however, it could be due to the presence of different impurities in the samples.

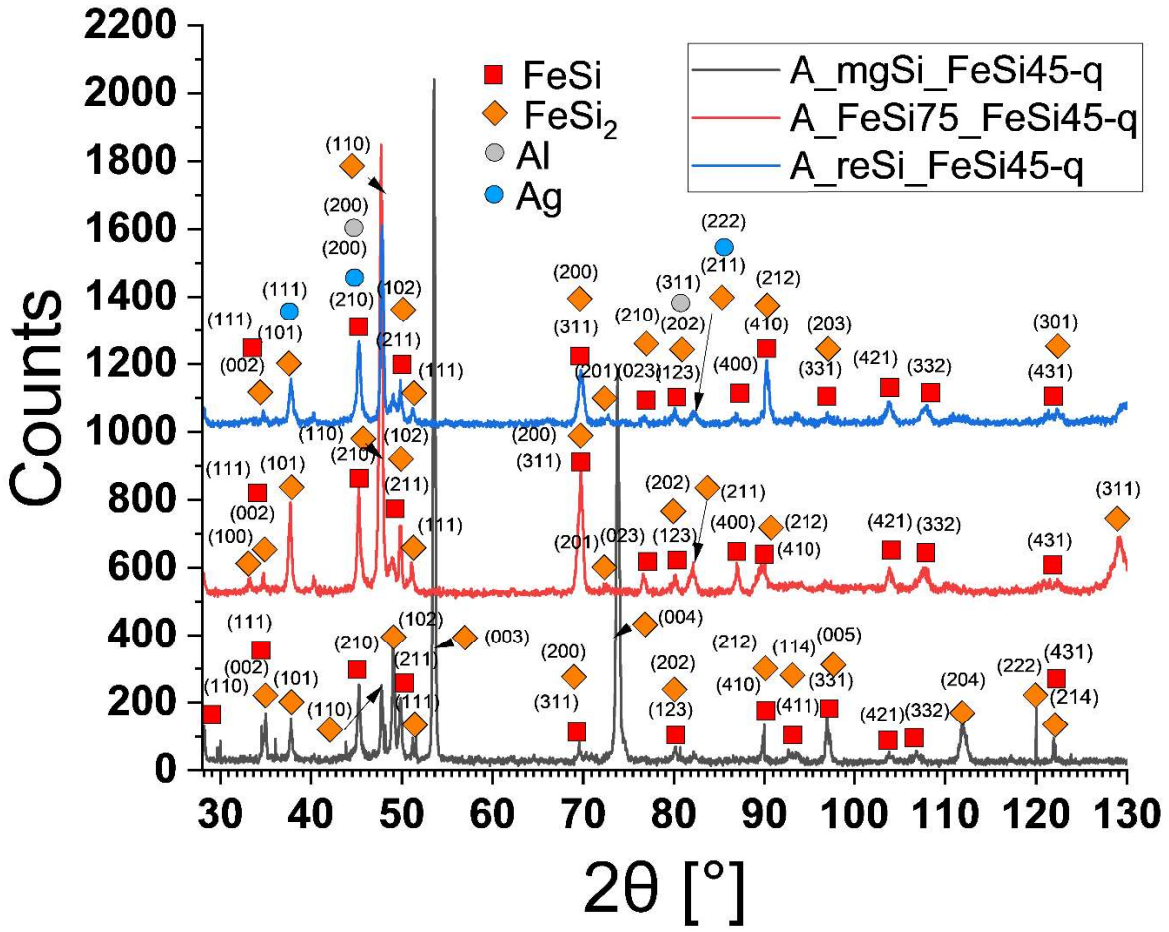

Figure 16: XRD patterns of FeSi samples prepared in Arc furnace with different sources of Si.

4.4 Impact of chemical and phase composition on hardness of FeSi

The harness of the prepared FeSi samples was evaluated and analysed to understand the impact of the change in silicon concentration, silicon source and fabrication procedure on the physical property. We selected hardness, as FeSi is usually crushed prior to use [2]. The hardness of the FeSi samples prepared in induction furnace having different percentages of Si and using different sources of Si are shown in figure 17. It was seen that the FeSi10 samples exhibited the lowest hardness values for all sources of Si. The hardness values increased for FeSi20 samples and again decreased for FeSi45 samples. The hardness results appear to be in agreement with the phases identified in samples using XRD. The FeSi20 samples exhibited the maximum hardness. This could be due to the presence of Fe_5Si_3 (Hexagonal) and Fe_2Si (trigonal) phases. The lower hardness of the FeSi10 samples could be owed to the presence of body centred cubic phases. Among the samples with different percentages of Si, the sample prepared using the reSi had lower hardness that those prepared with other sources, which could be related to the presence of marginally higher amount of Al. Nevertheless, this could reduce the energy consumption in processing and preparation of the FeSi samples prepared with reSi.

The samples prepared in arc furnace exhibited hardness values similar to those obtained for the samples prepared in induction furnace, with difference in values not more than ±10.

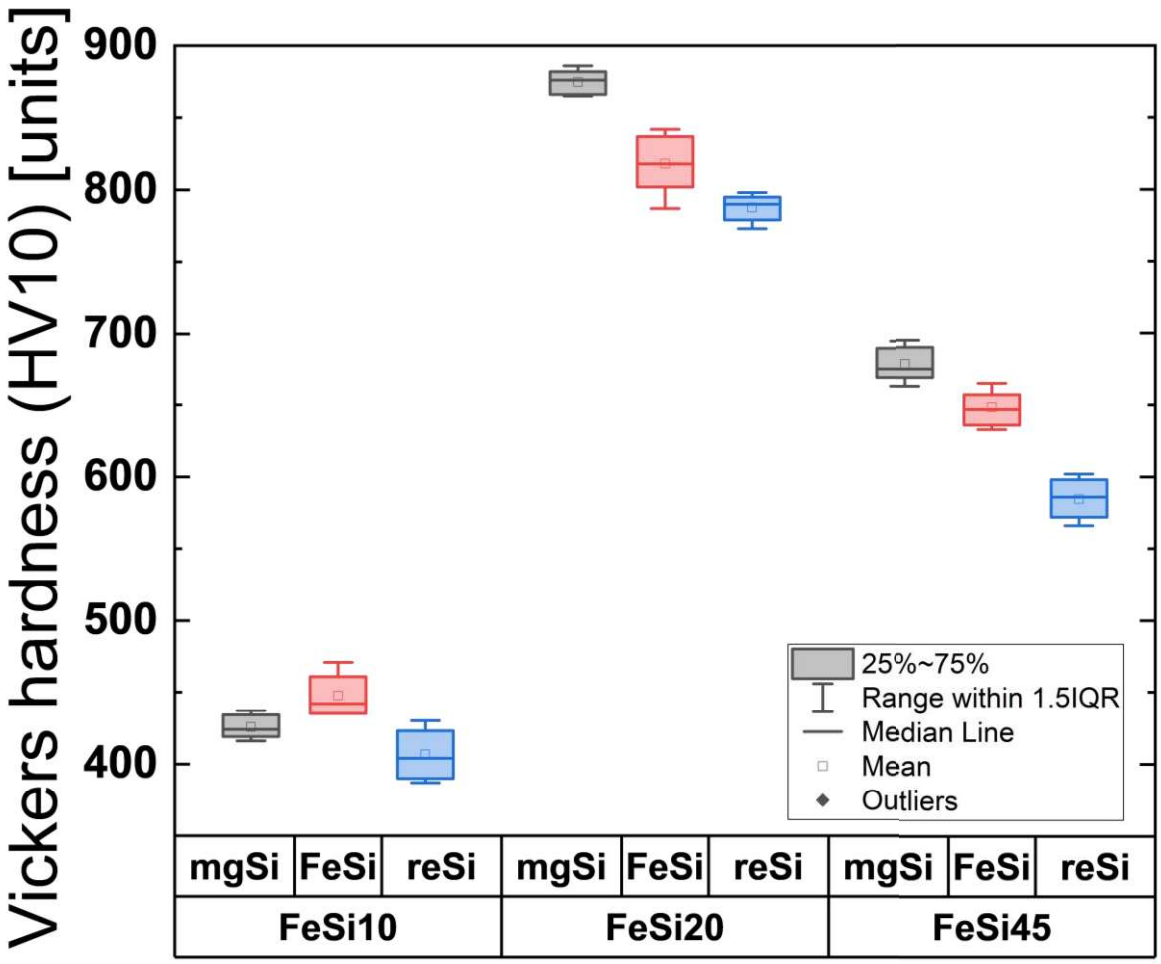

Figure 17: Hardness of FeSi samples determined by Vickers harness tester (HV10). The results here are shown only for the samples prepared in Induction furnace.

4. Conclusion

Increased deployment of silicon PV panels is a positive response to combat climate change. However, with increased deployment of PV panels, there is an urgent need to develop cost-effective and simple technologies for effective recycling of decommissioned or discarded Si PV panels. FeSi is a commercially important material and has multiple metallurgical applications. However, traditional production of FeSi usually involves use of carbonaceous sources and generates greenhouse gases and dust. In this work we have proposed using recycled Si originating from EOL Si PV panels for the production of FeSi. The recycled Si obtained from PV panels usually contain Ag and Al as major contaminants, however, together they account for less than 1% wt. if Si. Use of reSi for preparation of FeSi would not need any carbonaceous matter for reduction and could be prepared in induction furnaces requiring only electricity as the source of energy. Depending on the source of electricity generation (fossil fuels or renewables), the production of FeSi using reSi could potentially reduce the amount of greenhouse gases emitted during its production. In this work, samples were prepared using

three different sources of silicon (mgSi, FeSi75 and reSi) and containing different amount of Si (10, 20, 45). Two different types of furnaces (Induction and Arc) were used to prepare FeSi45 samples using different sources of Si. The samples prepared in Arc furnace were prepared under Ar atmosphere to evaluate the impact of oxygen in the processing environment. We analysed the microstructure using SEM and characterized the composition using EDS. In all cases, the morphology, microstructure and composition of the samples prepared using three different sources of Si were similar, except for the presence of Ag in the samples prepared using reSi. The microstructure was found to change with the change in Si concentration. For FeSi45 samples, two distinct phases could be identified, a Fe rich phase (Fe: Si ≈ 1:0.53) and a Si rich phase (Fe: Si ≈ 1:0.95). The Si in all the samples prepared in the induction furnace were less than the calculated amount by 2%-3% wt. (absolute), probably resulting from oxidation. The overall material loss in the samples prepared in the induction furnace was significantly more than for those produced in the arc furnace. This was found to be due to the oxidation of the volatile impurities contained in the samples, which could did occur in the induction furnace, due to absence of oxygen. XRD analysis of the phases revealed similar phases present for the samples with given silicon content prepared with different sources of Si. Mechanical evaluation of the hardness of the samples revealed that the samples prepared with reSi had lowest hardness for all concentrations of Si. The hardness values in general were lowest for FeSi10 samples, increased significantly for FeSi20 samples and decreased again for FeSi45 samples. This may result in lower energy consumption in crushing FeSi samples before use, resulting in further energy conservation. Samples prepared and arc and induction furnaces exhibited similar hardness values, hence there was no specific advantage of using oxygen free atmosphere. Therefore, induction furnace or arc furnaces operating in natural atmosphere would be more suitable to produce FeSi using reSi. While Ag in reSi is an additional component in the FeSi, it is < 0.1%wt of Si, resulting in overall <0.5% (wt.) in FeSi45 samples prepared using reSi. Additionally, there is a large interest in recovering Ag from the recycled Si solar cells [47–50] . Hence, the reSi could be treated first to remove Ag, and then used for producing FeSi. Recovery of Ag from reSi and using the processed reSi to produce FeSi could further improve the economy of recycling EOL Si PV panels. However, further research in the direction of environmental impact assessment and cost analysis of the proposed route is needed to prove the commercial viability of the process. Nevertheless, through this work it was found that reSi silicon could be an effective source for commercial production of FeSi.

Acknowledgements:

This research is part of the project No. 2022/45/P/ST5/02712, co-funded by the National Science Centre and the European Union Framework Programme for Research and Innovation Horizon 2020 under the Marie Skłodowska-Curie grant agreement No. 945339. For the purpose of Open Access, the author has applied a CC-BY public copyright license to any Author Accepted Manuscript (AAM) version arising from this submission.

Conflict of Interest statement

On behalf of all authors, the corresponding author states that there is no conflict of interest.

Bibliography

[1] M. Tilli, A. Haapalinna, Properties of silicon, INC, 2020. https://doi.org/10.1016/B978-0-12-817786-0.00001-3.

[2] M. Tangstad, Ferrosilicon and silicon technology, in: Handbook of Ferroalloys, Elsevier, 2013: pp. 179–220. https://doi.org/10.1016/B978-0-08-097753-9.00006-X.

[3] A. Müller, M. Ghosh, R. Sonnenschein, P. Woditsch, Silicon for photovoltaic applications, Materials Science and Engineering: B 134 (2006) 257–262. https://doi.org/10.1016/j.mseb.2006.06.054.

[4] J. Pastuszak, P. Węgierek, Photovoltaic Cell Generations and Current Research Directions for Their Development, Materials 15 (2022). https://doi.org/10.3390/ma15165542.

[5] H.H. Goh, C. Li, D. Zhang, W. Dai, C.S. Lim, T.A. Kurniawan, K.C. Goh, Application of choosing by advantages to determine the optimal site for solar power plants, Sci Rep 12 (2022) 1–16. https://doi.org/10.1038/s41598-022-08193-1.

[6] J. Khan, M.H. Arsalan, Solar power technologies for sustainable electricity generation - A review, Renewable and Sustainable Energy Reviews 55 (2016) 414–425. https://doi.org/10.1016/j.rser.2015.10.135.

[7] I. D'Adamo, M. Miliacca, P. Rosa, Economic Feasibility for Recycling of Waste Crystalline Silicon Photovoltaic Modules, International Journal of Photoenergy 2017 (2017) 1–6. https://doi.org/10.1155/2017/4184676.

[8] J. Wang, Y. Feng, Y. He, The research progress on recycling and resource utilization of waste crystalline silicon photovoltaic modules, Solar Energy Materials and Solar Cells 270 (2024) 112804. https://doi.org/10.1016/j.solmat.2024.112804.

[9] F. Corcelli, M. Ripa, S. Ulgiati, End-of-life treatment of crystalline silicon photovoltaic panels. An emergy-based case study, J Clean Prod 161 (2017) 1129–1142. https://doi.org/10.1016/j.jclepro.2017.05.031.

[10] S. Weckend, A. Wade, G. Heath, End-of-Life Management: Solar Photovoltaic Panels, 2016. https://www.irena.org/publications/2016/Jun/End-of-life-management-Solar-Photovoltaic-Panels (accessed September 8, 2023).

[11] A. Divya, T. Adish, P. Kaustubh, P.S. Zade, Review on recycling of solar modules/panels, Solar Energy Materials and Solar Cells 253 (2023). https://doi.org/10.1016/j.solmat.2022.112151.

[12] Y. Yu, X. Bai, S. Li, J. Shi, L. Wang, F. Xi, W. Ma, R. Deng, Review of silicon recovery in the photovoltaic industry, Curr Opin Green Sustain Chem 44 (2023). https://doi.org/10.1016/j.cogsc.2023.100870.

[13] R. FALKNER, The Paris Agreement and the new logic of international climate politics, Int Aff 92 (2016) 1107–1125. https://doi.org/10.1111/1468-2346.12708.

[14] K. Liu, Q. Tan, J. Yu, M. Wang, A global perspective on e-waste recycling, Circular Economy 2 (2023) 100028. https://doi.org/10.1016/j.cec.2023.100028.

[15] R. Ahirwar, A.K. Tripathi, E-waste management: A review of recycling process, environmental and occupational health hazards, and potential solutions, Environ Nanotechnol Monit Manag 15 (2021) 100409. https://doi.org/10.1016/j.enmm.2020.100409.

[16] P. Padhamnath, M. Ślęzak, M. Karbowniczek, Disposing End of Life PV Modules – Reusing, Recycling and Upcycling, in: EU PVSEC 2023, EUPVSEC, Lisbon, Portugal, 2023: pp. 001–008. https://doi.org/10.4229/EUPVSEC2023/5DV.2.62.

[17] G.A. Heath, T.J. Silverman, M. Kempe, M. Deceglie, D. Ravikumar, T. Remo, H. Cui, P. Sinha, C. Libby, S. Shaw, K. Komoto, K. Wambach, E. Butler, T. Barnes, A. Wade, Research and development priorities for silicon photovoltaic module recycling to support a circular economy, Nat Energy 5 (2020) 502–510. https://doi.org/10.1038/s41560-020-0645-2.

[18] R. Contreras Lisperguer, E. Muñoz Cerón, J. de la Casa Higueras, R.D. Martín, Environmental Impact Assessment of crystalline solar photovoltaic panels' End-of-Life phase: Open and Closed-Loop Material Flow scenarios, Sustain Prod Consum 23 (2020) 157–173. https://doi.org/10.1016/j.spc.2020.05.008.

[19] R. Contreras-Lisperguer, E. Muñoz-Cerón, J. Aguilera, J. de la Casa, A set of principles for applying Circular Economy to the PV industry: Modeling a closed-loop material cycle system for crystalline photovoltaic panels, Sustain Prod Consum 28 (2021) 164–179. https://doi.org/10.1016/j.spc.2021.03.033.

[20] G. Thomassen, J. Dewulf, S. Van Passel, Prospective material and substance flow analysis of the end-of-life phase of crystalline silicon-based PV modules, Resour Conserv Recycl 176 (2022) 105917.

[21] P. Dias, P. Dias, H. Veit, Recycling crystalline silicon photovoltaic modules, Emerging Photovoltaic Materials: Silicon & Beyond (2018) 61–102.

[22] P. Su, Y. He, Y. Feng, Q. Wan, T. Li, Advancements in end-of-life crystalline silicon photovoltaic module recycling: Current state and future prospects, Solar Energy Materials and Solar Cells 277 (2024). https://doi.org/10.1016/j.solmat.2024.113109.

[23] M. Akhter, A. Al Mansur, M.I. Islam, M.S.H. Lipu, T.F. Karim, M.G.M. Abdolrasol, T.A.H. Alghamdi, Sustainable Strategies for Crystalline Solar Cell Recycling: A Review on Recycling Techniques, Companies, and Environmental

Impact Analysis, Sustainability (Switzerland) 16 (2024). https://doi.org/10.3390/su16135785.

[24] W. Palitzsch, I. Rover, J. Lee, Y. Yook, Single crystalline Si ingot by use of recycled silicon as an example for circular economy, EUPVSEC 2020 (2020).

[25] A. Derbouz Draoua, B. Martel, S. Dubois, C. Audoin, M. Sérasset, A. Fauveau, H.S. Radhakrishnan, J. Denafas, L. Petreniene, N. Severino, On the Fabrication of Solar Cells Based on Newly Produced Recycled Silicon Feedstocks From CABRISS-A Comparative Study Between Material Properties and Solar Cell Performances, in: EU PVSEC 2017-33rd European Photovoltaic Solar Energy Conference and Exhibition, WIP, 2017: pp. 483–487.

[26] B. Jung, J. Park, D. Seo, N. Park, Sustainable System for Raw-Metal Recovery from Crystalline Silicon Solar Panels: From Noble-Metal Extraction to Lead Removal, ACS Sustain Chem Eng 4 (2016) 4079–4083. https://doi.org/10.1021/acssuschemeng.6b00894.

[27] D. Mao, S. Yang, L. Ma, W. Ma, Z. Yu, F. Xi, J. Yu, Overview of life cycle assessment of recycling end-of-life photovoltaic panels: A case study of crystalline silicon photovoltaic panels, J Clean Prod 434 (2024) 140320. https://doi.org/10.1016/j.jclepro.2023.140320.

[28] F.C. Okoroigwe, E.C. Okoroigwe, O.O. Ajayi, S.N. Agbo, J.N. Chukwuma, Photovoltaic Modules Waste Management: Ethical Issues for Developing Nations, Energy Technology 8 (2020). https://doi.org/10.1002/ente.202000543.

[29] S. Mahmoudi, N. Huda, M. Behnia, Environmental impacts and economic feasibility of end of life photovoltaic panels in Australia: A comprehensive assessment, J Clean Prod 260 (2020) 120996. https://doi.org/10.1016/j.jclepro.2020.120996.

[30] P. Nain, A. Kumar, Metal dissolution from end-of-life solar photovoltaics in real landfill leachate versus synthetic solutions: One-year study, Waste Management 114 (2020) 351–361. https://doi.org/10.1016/j.wasman.2020.07.004.

[31] D. Hawezy, The influence of silicon content on physical properties of non-oriented silicon steel, Materials Science and Technology (United Kingdom) 33 (2017) 1560–1569. https://doi.org/10.1080/02670836.2017.1295519.

[32] A. Selema, M. Beretta, M.N. Ibrahim, J. Verwimp, M. Rombouts, J. Vleugels, L.A.I. Kestens, P. Sergeant, Material Engineering of 3D-Printed Silicon Steel Alloys for the Next Generation of Electrical Machines and Sustainable Electromobility, J Magn Magn Mater 584 (2023) 171106. https://doi.org/10.1016/j.jmmm.2023.171106.

[33] N. Haque, T. Norgate, Estimation of greenhouse gas emissions from ferroalloy production using life cycle assessment with particular reference to Australia, J Clean Prod 39 (2013) 220–230. https://doi.org/10.1016/j.jclepro.2012.08.010.

[34] G. Sævarsdottir, H. Kvande, T. Magnusson, Greenhouse Gas Emissions from Silicon Production -Development of Carbon Footprint with Changing Energy Systems, SSRN Electronic Journal (2021) 27–29. https://doi.org/10.2139/ssrn.3926088.

[35] L. Riva, G.R. Surup, T.V. Buø, H.K. Nielsen, A study of densified biochar as carbon source in the silicon and ferrosilicon production, Energy 181 (2019) 985–996. https://doi.org/10.1016/j.energy.2019.06.013.

[36] N. Nandakumar, J.W. Rodriguez, P. Padhamnath, N. Nampalli, A.G. Aberle, S. Duttagupta, Large-area monoPoly solar cells on 110 μm thin c–Si wafers with a rear n+ poly-Si/SiOx stack deposited by inline plasma-enhanced chemical vapour deposition, Progress in Photovoltaics: Research and Applications 31 (2023) 360–368.

[37] J. Haunschild, J. Broisch, I. Reis, S. Rein, Cz-Si wafers in solar cell production: Efficiency-limiting defects and material quality control, Photovoltaics International 15 (2012) 40–46.

[38] H.A. Wriedt, W.B. Morrison, W.E. Cole, The solubility of silver in γ-Fe, Metallurgical Transactions 4 (1973) 1453–1456.

[39] F. Rollert, N.A. Stolwijk, H. Mehrer, Solubility, diffusion and thermodynamic properties of silver in silicon, J Phys D Appl Phys 20 (1987) 1148.

[40] E.J. Freise, A. Kelly, R.B. Nicholson, Guinier-preston zones in an aluminium-silver alloy, Acta Metallurgica 9 (1961) 250–255.

[41] K. Hirano, Y. Takagi, On the Solid Solubility of Silver in Aluminium, J Physical Soc Japan 9 (1954) 730–735.

[42] T. Urban, A. Mette, J. Heitmann, Influence of silver-aluminium alloy at solar cell rear side on series resistance and open circuit voltage, Energy Procedia 92 (2016) 236–241.

[43] P. Padhamnath, W.-J. Choi, G. De Luna, J.D. Arcebal, A. Rohatgi, Design, development and analysis of large-area industrial silicon solar cells featuring a full area polysilicon based passivating contact on the rear and selective passivating contacts on the front, Solar Energy Materials and Solar Cells 256 (2023) 112351.

[44] P. Padhamnath, W.-J. Choi, G. De Luna, J.D. Arcebal, A. Rohatgi, A.G. Aberle, Design and development of front and back contact solar cells with selective poly-Si passivating contact on the front and local Al contact on the rear, Solar Energy Materials and Solar Cells 269 (2024) 112759.

[45] T.I. Sigfússon, Ö. Helgason, Rates of transformations in the ferrosilicon system, Hyperfine Interact 54 (1990) 861–867. https://doi.org/10.1007/BF02396141.

[46] Q.C. Hom, C.L. Nassaralla, R.W. Heckel, Microstructural Study of Granulated Ferrosilicon with 75wt% Silicon, in: The Proceedings of ·/NFACON 8, Beijing, 1998. https://www.pyrometallurgy.co.za/InfaconVIII/126-Horn.pdf (accessed January 18, 2025).

[47] L.S.S. de Oliveira, M. Lima, L.H. Yamane, R.R. Siman, Silver recovery from end-of-life photovoltaic panels, Detritus 10 (2020) 62–74.

[48] Q. Han, Y. Gao, T. Su, J. Qin, C. Wang, Z. Qu, X. Wang, Hydrometallurgy recovery of copper, aluminum and silver from spent solar panels, J Environ Chem Eng 11 (2023) 109236.

[49] S. Rout, P. Jana, C.R. Borra, M.A.R. Önal, Unlocking silver from end-of-life photovoltaic panels: A concise review, Renewable and Sustainable Energy Reviews 210 (2025) 115205.

[50] P. Dias, S. Javimczik, M. Benevit, H. Veit, A.M. Bernardes, Recycling WEEE: Extraction and concentration of silver from waste crystalline silicon photovoltaic modules, Waste Management 57 (2016) 220–225.

Investigation of Ferrosilicon produced with Si recovered from end-of-life photovoltaic panels.

Filip Kuśmierczyk, Mateusz Kopyściański, Adarsh Rai, Tomasz Kozieł, Marcin Goły, Agnieszka Kopia, Piotr Migas, Mirosław Karbowniczek, Pradeep Padhamnath*

AGH University of Krakow, al. Adama Mickiewicza 30, 30-059 Kraków, Poland

*ppadhamnath@agh.edu.pl

Graphical Abstract

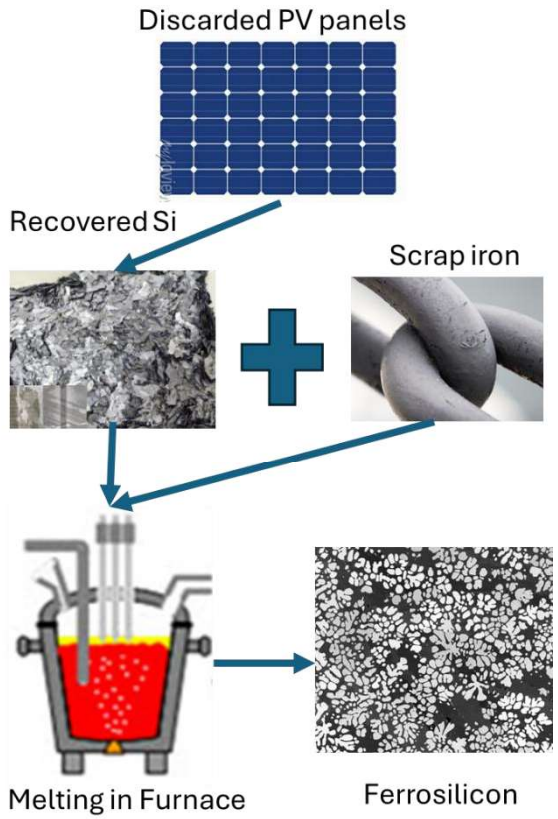

Figure showing the overall process of producing ferrosilicon from silicon recovered from end-of-life silicon photovoltaic panels used in this work.